Integrating experiments and models to unravel interactions between soil organic matter and enhanced weathering.

Arthur Vienne[1] , Tom Cox[1], Harun Niron[1], Bertrand Guenet[2], Reinaldy Poetra[3], Laura Steinwidder[1], Charline Vandenhove[1], Sara Vicca[1]

[1] Biobased Sustainability Engineering (SUSTAIN), Department of Bioscience Engineering, University of Antwerp, Antwerp, Belgium.
[2] Laboratoire de Geologie ENS, PSL Research University, CNRS, UMR 8538, IPSL, Paris, France
[3] Department of Earth System Sciences, Universität Hamburg, Bundesstraße 55, 20146 Hamburg, Germany

Corresponding Author: Arthur Vienne (arthur.vienne@uantwerpen.be)

KEYWORDS: Basalt, Enhanced weathering, soil organic matter, specific surface area, MRV

ABSTRACT

Enhanced weathering (EW) aims to accelerate rock dissolution to sequester atmospheric CO_2. Here, we investigated key uncertainties in modelling C sequestration through EW by comparing a coupled inorganic-organic geochemical model against soil measurements and soil CO_2 efflux from a 389-day mesocosm experiment with soils amended with varying manure, basalt and dunite inputs.

Silicate amendments did not enhance dissolved inorganic C leaching or significantly increase pedogenic carbonate accumulation. PHREEQC simulations indicate that base cations preferentially precipitated as secondary clays instead of carbonates, thereby inhibiting inorganic CO_2 removal. Sequential extractions suggest that Al, Fe and base cations

were retained in soils through cation exchange, adsorption to (hydr)oxides and organic matter, with model results indicating additional retention in secondary clays. Cumulative soil CO_2 efflux and was not significantly altered by rock amendments.

Higher organic matter addition did not increase the release of elements from basalt (and even reduced leached K and Fe), while decreasing the reactive surface area of basalt, indicating a counteractive effect of organic matter on rock weathering. Cumulative soil CO_2 efflux did not differ significantly among silicate-amended treatments, consistent with PHREEQCENTURY simulations. The model predicted limited treatment effects on CO_2 efflux in this soil due to minor changes in soil pH and moisture and limited stabilization of organic C that may correspond to MAOM formation.

1. Introduction

To achieve the well below 2 °C warming target of the Paris Agreement, carbon dioxide removal (CDR) approaches must be deployed alongside conventional emission-reduction strategies rather than as stand-alone solutions (IPCC, 2023). Enhanced weathering (EW) is an emerging CDR technique, which has attracted significant attention in recent years. Global CDR potentials on cropland were estimated to exceed several gigatons per year (Strefler et al., 2018). CO_2 is sequestered by reaction of silicate (or carbonate) rock with H_2O and CO_2, increasing HCO_3^- and base cations (Na, K, Mg and Ca) in solution (as illustrated in **Reaction 1** for forsterite, the Mg-endmember of olivine). Dissolved base cations and HCO_3^- can subsequently precipitate as carbonates, halving CDR as 50% of the initially captured CO_2 is degassed (**Reaction 2**). These reactions already sequester CO_2 in natural geological systems, yet at a slow rate. Natural weathering can be accelerated by grinding rock to fine powders, which drastically increases specific surface area (SSA) and therefore CDR rates (Schuiling & Krijgsman, 2006).

$$Mg_2SiO_4 + 4\ CO_2\ (g) + 4\ H_2O \rightarrow 2\ Mg^{2+} + 4\ HCO_3^- + H_4SiO_4 \qquad \textbf{Reaction 1}$$

$$4\ HCO_3^- + 2\ Mg^{2+} \rightarrow 2\ MgCO_3 + 2\ H_2O + 2\ CO_2\ (g) \qquad \textbf{Reaction 2}$$

Dunite, mainly composed of olivine (>90% $(Mg,Fe)_2SiO_4$), and basalt are considered promising feedstocks for EW because of their global abundance and high CDR potential. Basalts contain a mixture of minerals, including olivine as well as pyroxene and plagioclase minerals. Based on their base cation content, CDR potentials of dunite and basalt have been estimated to approximate 1100 and 300 kg CO_2 t $rock^{-1}$ respectively (Strefler et al. (2018)). These values represent maximum CDR potentials, assuming no base cation uptake by carbonate precipitation, by secondary minerals or other mechanisms.

The first models that predicted the CDR potential of EW were only constrained by rock weathering rates derived from lab-scale rock dissolution experiments (Palandri & Kharaka, 2004). Recently, more complex, geochemical reactive transport models have been developed to deal with the complex environment of soils, for example using THOUGHREACT or PHREEQC software (Beerling et al., 2020; Kelland et al., 2020; Lewis et al., 2021; Schwartz, 2022; Vienne et al., 2022). The CDR rates predicted by EW models are, however, sensitive to several key variables including CO_2 pressure, secondary mineral formation, specific surface area (SSA) and soil organic matter (SOM) decomposition, which could all be influenced by interactions between rocks and soil organic C (SOC) in soils.

Soil organic matter decomposition is a major contributor to the soil CO_2 pressure, which enhances carbonic acid formation and lowers soil pH, thereby stimulating rock weathering (Amann et al., 2022). Moreover, as pH decreases, OH^- and CO_3^{2-} ions decrease, limiting the formation of

hydroxide-bearing secondary minerals and pedogenic carbonates. Secondary minerals influence the dissolution of primary minerals by incorporating or sorbing ions and altering porewater chemistry (Lewis et al., 2021). By removing ions from solution, secondary mineral formation can maintain undersaturation, further stimulating mineral dissolution. Surface passivation by precipitated phases, on the other hand, can reduce dissolution rates (Hellmann et al., 2013; Oelkers et al., 2018). The type of secondary minerals present is important in this regard. For example, Lewis et al. (2021) showed that whether Al forms amorphous or crystalline $Al(OH)_3$ (gibbsite) strongly impacts Al scavenging and aluminosilicate weathering, and hence also CDR.

When rocks weather with CO_2 and H_2O, dissolved HCO_3^- and base cations increase (e.g**. reaction 1**). Subsequently, the base cations can become incorporated into secondary minerals resulting in protons release (illustrated here with the formation of chlorite in **Reaction 3**), which can then react with carbonates (CO_3^{2-} and HCO_3^-) to form CO_2 and H_2O, hence inhibiting inorganic CO_2 removal.

$$5Mg^{+2} + 2Al^{+3} + 3H_4SiO_4 + 6\ H_2O \rightarrow Mg_5Al_2Si_3O_{10}(OH)_8 + 16H^+ \qquad \textbf{Reaction 3}$$

A third key parameter is the surface area of rocks, which can be determined experimentally through Brunauer Emmett Teller (BET) adsorption measurement (BET-SSA) or can be modelled based on particle size. This modelled or geometric SSA is easier to determine as it only requires information about particle size distribution (Rinder & von Hagke, 2021), yet can be an order of magnitude smaller than those determined through gas absorption (Renforth et al., 2015). In addition, changes in rock porosity over time due to adsorption of organics on surfaces may lead to erroneous estimates of actual SSA.

Last, rock dissolution may influence the decomposition of SOM. Increases in pH can stimulate decomposition while cation release and secondary mineral formation can stimulate SOM

stabilization (Vicca et al., 2022). In peatlands, Klemme et al., (2022) simulated that increased pH after rock amendment can increase decomposition rates and losses SOC. On the other hand, secondary minerals such as clays or Fe-/Al hydroxides can adsorb dissolved organic C (DOC) and thus protect SOC from microbial respiration (Kothawala et al., 2009), potentially increasing SOC stocks (Niron et al., 2024; Vicca et al., 2022; Xu et al., 2024). These EW-SOC interactions are usually not considered in EW models (Kelland et al., 2020; Lewis et al., 2021; Schwartz, 2022), yet recent studies indicate that interactions with SOC are critical to understand to climate impact of EW (Boito et al., 2025; Lei et al., 2025; Steinwidder et al., 2025; Vicca et al., 2022; Xu et al., 2024, 2025).

In this study, we aim to integrate experimental results with model predictions, while gaining insights into interactions and model uncertainties. We conducted a mesocosm experiment testing the interactions between silicates and organic matter for two rock types: basalt and dunite. To assess the influence of SOC, two amounts of manure were added in separate treatments. Key investigated parameters include leached elements, leached dissolved inorganic C (DIC), soil inorganic C (SIC), secondary mineral formation, rock surface area and soil CO_2 efflux (SCE) in unplanted soils. In addition, we compared our measurements with PHREEQC model predictions. To this end, we coupled PHREEQC to an established organic C model (Century) resulting in a coupled model: PHREEQCENTURY.

2. Material and Methods

2.1 Experimental set-up

In total, our experiment lasted approximately 1 year and 1 month (389 days). The experiment consisted of 35 mesocosm (56 × 39 × 28 cm—area: 0.22 m²). On November 22, 2022, the control pots were filled with 30 kg of acidic sandy-loam soil. This soil was then mixed with 0.55 kg of

cow manure using a concrete mixer to increase the SOC to 1%, ensuring sufficient CO_2 production in the soils. Additionally, to create a 3% SOC soil, we added 3.35 kg of cow manure to achieve the desired SOC level. The mesocosms were then amended with rock powders of different particle sizes (F = fine, M = medium, C = coarse). Treatments included basalt, dunite, and controls without rock powder amendment (B, D, C). Basalt (type DURUBAS) was sourced from Rheinischen Provinzial- Basaltund Lavawerke (RBPL) applied at 100 t ha^{-1}, while dunite was delivered by Sibelco and applied at a rate of 5 t ha^{-1}. An overview of the treatments is provided in Table 1. The fine basalt treatment with 1% SOC was also included in the study on the effect of B. subtilis addition presented in Niron et al (2024). Details on the composition of the utilized soil and manure (which was alkaline) for relevant parameters can be found in **Table 2**, while rock characterization can be found in **Table 3.**

Table 1: Overview of experimental treatments.
*Diameter larger than 90% of particles

Treatment code	**C1**	**FB1**	**C 3**	**FB3**	**CB3**	**FD3**	**MD3**	**CD3**
silicate type	/	Basalt	/	Basalt	Basalt	Dunite	Dunite	Dunite
ton silicate ha^{-1}	0	100	0	100	100	5	5	5
amount of silicate (kg) per mesocosm	0	2.2	0	2.2	2.2	0.11	0.11	0.11
amount of manure (kg) per mesocosm	0.55	0.55	3. 35	3.35	3.35	3.35	3.35	3.35
D90 particle size (µm)*	/	292	/	292	670	71	278	1030
Initial SOC (%)	1	1	3	3	3	3	3	3

Table 2: Properties of rainwater, unamended soil and manure. Adapted from Niron et al. (2024).
*BD= Below the detection limit.

Sample	pH (in H2O 2.5 mL:1g for solids)	EC (µS/cm)	Solid inorganic carbon (%)	Texture
Rainwater	6.960 ± 0.01	130.35 ± 1.15	/	/
Soil	5.585 ± 0.234	84.775 ± 33.315	*BD	Sandy loam (61% sand, 4% clay, 35 % silt)
Manure	8.213 ± 0.118	6997 ± 619.2	0.1705	/

Table 3: XRD data of the applied Durubas basalt and dunite rock.

XRD				XRF		
Mineral phase	**Durubas basalt (wt%)**	**Mineral phase**	**Dunite (wt%)**	**Oxide**	**Durubas Basalt (wt%)**	**Dunite (wt%)**
Augite	50	Olivine*	86.6	SiO_2	44.6	41.6
Plagioclase	35	Clinopyroxene	1.2	Fe_2O_3	11.7	7.3
Olivine	5	Orthopyroxene	4.4	CaO	10.8	0.4
Illite	5	Chlorite	2.4	MgO	12.9	47.9
Chlorite	5	Serpentine	2.3	Al_2O_3	11.5	0.8
		Talc	0.4	Na_2O	2.6	0.0
		2:1 layer silicates	2.6	TiO_2	2.3	0.0
				K_2O	0.7	0.0
				P_2O_5	0.9	0.0
				MnO	0.2	0.1

*The mineralogy of olivine approximates the Mg-endmember (forsterite, Mg_2SiO_4) (Amann et al., 2022).

During the first 130 days after amendment, temperature and soil moisture were continuously monitored with sensors buried at 12 cm depth (CS655, Campbell Scientific, USA). Afterwards, due to limited sensor availability, temperature and moisture were registered biweekly. As the

experiment took place indoors, temperature fluctuations in time were minor (although temperature was higher during summer). Temperature and soil moisture are provided in **Fig. S1.** Each mesocosm was watered with 1 L of rainwater per week, corresponding to 223 mm $year^{-1}$. Rainwater was collected from a local roof and analyzed for pH, EC and elements (**Table 2** and **Table S1).** The percolated water (hereafter named "leachate") was collected in a container below the mesocosms.

In order to investigate changes in SSA and carbonates in rock powders, mesh bags (140 × 157 mm, 45 μm pore size, Top Zeven B.V., NLD) filled with pure basalt and dunite were placed horizontally in each mesocosm at 5–6 cm depth. After 130 days, about 20g of rock powder was sampled from mesh bags, which were then placed back into the soil. Similar disturbance activity was performed for the control soils without mesh bags to account for potential disturbance effects. After 392 days, mesh bags were sampled in an identical way.

2.2 Sampling and measurements

Leachate samples were collected biweekly and filtered (0.45 μm PET filter, Merck, USA) for further analyses. pH and conductivity were measured with a pH/conductometer (914, Methrohm, CHE). Elemental (Ca, Mg, K, Na, Fe, Al, Si, P, and Ni) analyses were measured on three occasions (days 14, 56, and 113 corresponding to leachates of weeks 0–2, 6–8, and 14–16, respectively). Elemental analysis was performed with ICP-OES (iCAP 6300 duo, Thermo Scientific, USA) for Ca, Mg, K, and Na and with HR-ICP-MS (Element 2, Thermo Scientific) for other elements using acidified samples (19:1–2%- HNO_3:Sample, TraceMetal Grade, Fisher Chemical). Calibration standards were prepared using a multi-element standard (CPAChem). Alkalinity analysis was performed using a continuous flow analyzer (SAN++, Skalar, NLD). DIC and DOC were measured with a catalytic combustion-based TOC analyzer (FormacsHT, Skalar, NLD) and

initially analyzed biweekly until day 130. While the last soil water sample for elemental analyses other than C was taken at day 130 of the experiment, monitoring of DIC and DOC continued monthly until day 389.

Two types of solid material were analyzed for each mesocosm: silicate–soil mixtures and unmixed silicates in mesh bags, both sampled after 130 days. Dissolved element losses (Na, K, Ca, Mg, Fe, Al, Si) were assessed by measuring leaching and by sequential extractions (after Tessier et al., 1979) to quantify retention in four soil pools: exchangeable, carbonate-associated, reducible (hydroxide-associated), and oxidizable (SOM-associated) (Table 4; Niron et al., 2024).

Table 4: Modified version of the sequential extraction procedure from Tessier et al. (1979).

Fraction	Solvent	Conditions
Exchangeable	1 M $BaCl_2$, pH 7.0, 8 ml	Room temperature, 1 h, continuous agitation
Carbonate bound	1M NaOAc, pH 5.0 (adjusted with HOAc), 8 ml	Room temperature, 4 h, continuous agitation
Reducible	0.04 $NH_2OH.HCl$ in 25% (v/v) HOAc, 20 ml	96°C, 6 h, occasional agitation
Oxidizable	(i) 0.02 M HNO_3, 3 ml + 30% H_2O_2, pH 2.0, 5 ml (adjusted with HNO_3) (ii) 30% H_2O_2, pH 2.0 (adjusted with HNO_3), 3 ml (iii) 3.2 M $NH_4(CH_3COO)$, 5 ml in 20% (v/v) HNO_3 + H_2O, 4 ml	(i) 85°C, 2 h (ii) 85°C, 3 h (iii) RT, 0.5 h, continuous agitation

Carbonates were measured in mesh-bags filled with silicates and in the bulk soil. Calcimetry was applied only to pure rock powders in mesh bags (methodology, see supplement, section 4). In the bulk soil, Carbonate-associated cations were quantified from base cations in the Tessier carbonate-associated soil pool, similar to Larkin et al. (2022). After extraction of 1 g of sample with 8 mL 1M $BaCl_2$, samples were centrifuged at 3000 rotations per minute (rpm) for 5 minutes, washed once with 20 mL of DI water, centrifuged at 3000 rpm for 5 minutes again and the pellet was re-

extracted using 8 mL of 1M Na acetate adjusted to pH 5.0 with acetic acid. Through charge balance, for every mol of Ca and Mg in the acetate extracts, 1 mol of SIC was assumed to be extracted. The extract volume was 8 mL in this case (**Equation 1**).

$$\Delta SIC[\%] = \frac{\left((\Delta Ca + \Delta Mg + \Delta Fe)\left[\frac{mol}{L}\right] + \left(\frac{\Delta K}{2}\right)\left[\frac{mol}{L}\right]\right) * Extract\ Volume\ [L] * 12\left[\frac{gSIC}{mol\ SIC}\right] * 100}{Soil\ mass\ [g\ soil]} \quad (1)$$

SSA can be simulated based on particle size distribution, yet changes in rock porosity over time may lead to erroneous estimates of actual SSA. We therefore measure SSA using gas adsorption: BET-SSA of mesh-bag samples was measured with a Quantachrome Autosorb iQ using N_2 adsorption (multi-point, 5 points, 77 K). Samples of the same treatment were pooled to reduce cost and time, degassed at 300 °C for 200 min, and measured in triplicate with frequent reference checks (BAM-PM-102, Bundesanstalt für Materialforschung und -prüfung, Germany) for quality control. Silicate particle size was analyzed with a Mastersizer 2000 and Hydro 2000G after sieving at 1 mm (for a detailed particle size distribution, see **Table S4**). Coarse dunite contained particles >1 mm, quantified separately by manual sieving.

In addition to the abovementioned liquid and solid analyses, SCE was measured using a cylindrical chamber (0.98 L, 0.0082 m²), which fitted on a collar that was placed in the soil. The chamber was connected to a portable gas analyzer (Picarro, G2201- i, CA US) for approximately 90 seconds to monitor the changes in CO_2 concentration (ppmv/s). CO_2 was measured on 32 occasions (i.e. on average once every 12 days).

2.3 Statistical analyses

For time-series variables (e.g., SCE, leachate chemistry), repeated-measures mixed models were fitted using lmer (lme4 package), with mesocosm as random factor, and significances was assessed with Anova (car package). Tessier soil fractions, which were measured once, were analyzed using multiple linear regression followed by Anova.

To address different questions with appropriate factorial structures, we analyzed two subsets of the data. Treatments C1, FBS1, C3, and FB3 were used to test basalt and SOM effects in a full factorial design (1 vs. 3% SOC) to assess their interaction. To examine particle-size effects and the qualitative effect of rock type, we analyzed the 3% SOC treatments only (FB3, CB3, FD3, MD3, CD3, C3). In this dataset, "rock" was treated as a factor with three levels ("none," "basalt," or "dunite"). Pairwise comparisons were performed using emmeans (Tukey method). To test potential interactions with time, we used the functions emtrends and pairs.

To evaluate treatment effects independent of potential differences in temperature and SWC, the time series for SCE were first fitted to temperature and soil moisture using a multiple linear regression (lmer) of CO_2 flux ($\mu mol\ m^{-2}\ s^{-1}$) against temperature and soil moisture ($CO_2 = a + b\ Temperature + c\ SWC + d\ SWC^2$; as in Niron et al. (2024)). Residuals of this model were then used as dependent variable to test for the effect of basalt, dunite and SOC in the two subsets of the data as described above. Statistical significance was set at $p < 0.05$, and all analyses were performed in RStudio (v2023.9.1.494).

For graphical representation only, delta values (Δ) were calculated as the difference between an amended soil (basalt or dunite treatment) and the respective control soil (C1 for FB1 and C3 for FB3, CD3, MD3 and FD3). These delta values were not included in the statistical analyses.

2.4 Model structure and parameterization

In order to simulate the interaction between weathering reactions and SOC, we combined the inorganic PHREEQC model (based on the work of Kelland et al. (2020), Vienne et al. (2022) and Lewis et al. (2021)) with an organic module (based on the 'Century model' with DOC adsorption by Fe-/Al-hydroxides (Camino-Serrano et al., 2018)(**Figure 1**). Note that Century is a plant-soil model (Dimassi et al., 2018) and only the soil module was used in this decomposition experiment with bare soil. The Century SOC model divides the C input into a metabolizable soil pool and a structural soil pool based on C/N and lignine content of the input organic matter. These pools then decompose into three C pools (active, slow, and passive) each with distinct turnover rates. The active/slow pool conversions are influenced by the clay content of the soil; In addition, mineral surfaces (Fe- and Al-hydroxides) increase the maximal DOC adsorption capacity (Qmax) and transfer active C into adsorbed DOC, unavailable for microbial respiration (**Figure 1**).

In the weathering module of the model, plagioclase in basalt was simulated as the Ca-Na intermediate labradorite, while olivine in basalt was simulated as an Fe-Mg olivine intermediate and we ensured the stoichiometry of simulated basalt matched the stoichiometry derived from XRF data.

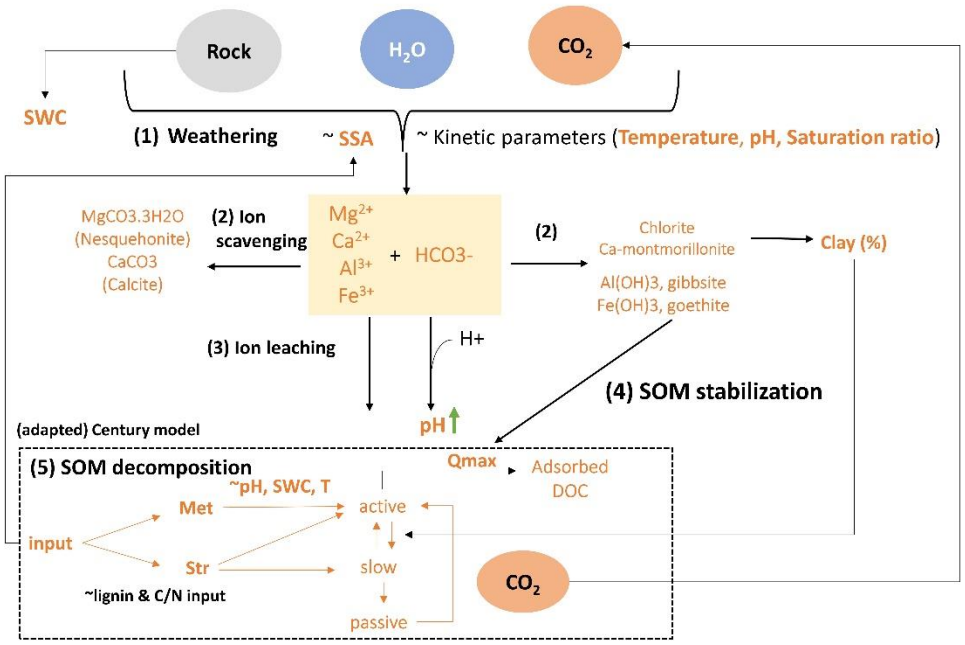

Figure 1: Overview of the coupled PHREEQC / Century (PHREEQCentury) model. Variables in orange are dynamic and thus change at every timestep. SWC = Soil water content, SSA = specific surface area, Qmax = Maximum DOC sorption capacity, Met= metabolizable soil pool, Str= Structural soil pool.

The mesocosms were simulated as single well mixed batches/volumes. Initial values of the pore water composition was set to observed concentrations of the soil-leachate. Daily experimental inputs of SWC, SCE, SSA, and temperature were provided, with SSA and SCE fitted to experimental values for each treatment. The time step of the model was daily. "Temperature and moisture effects on SOM decomposition rates were taken into account with a classical Q10 function for temperature (Q10 = 2) and Gompertz relationship for soil moisture (Sierra et al., 2015).

The pCO_2 at mean soil depth was calculated from observed SCE via Fick's law (Roland et al., 2015; Vienne et al., 2022) and pH was simulated by PHREEQC based on pCO_2 and total alkalinity. To modify SOM decomposition with pH, we introduced a pH modifier based on Leifeld et al.'s (2008) S-shaped pH modifier (0 at pH 2, 1 at pH 8). Secondary minerals (Al/Fe-hydroxides,

gibbsite, Ca-montmorillonite, goethite, chlorite) were included in the equilibrium phase function with precipitation thresholds based on saturation index (SI), allowing for oversaturation (Knapp & Tipper (2022); Kelland et al., 2020). Minerals dissolved when $SI < 0$ and precipitated when $SI \geq 0$. For Mg- and Ca-carbonates (nesquehonite, calcite) we set a precipitation threshold $SI \geq 0$ or $SI \geq 1$ to precipitate in initial simulations. Based on comparison with observations, we used a $SI \geq 1$ threshold for carbonate precipitation in the eventual simulations. DOC adsorption to Fe/Al-hydroxides was simulated sensu Camino-Serrano et al (2018), with Qmax calculated from simulated Fe/Al hydroxides with the relation from (Kothawala et al (2009), table 4). Clay mass fractions (based on the mass of chlorite, Ca-montmorillonite) were dynamically updated, affecting Century active/slow pool C conversions. All simulations were performed in R and phreeqc, making use of the phreeqc R-package (version 3.7.6)

3. Results

3.1 Inorganic CO_2 removal

3.1.1 Leachate concentrations

Leaching of DIC did not significantly increase after rock amendment (**Figure 2**). While leaching of DIC, DOC, TA and base cations was on average higher in treatment FB1 relative to the control C1, we observed no significantly positive basalt effects on leaching. Furthermore, basalt and dunite significantly decreased leachate Al (both $p<0.01$ **Figure 2, Table S2)**. Dunite also significantly decreased leached K ($p=0.02$). Rock particle size did not significantly affect leaching of elements. Increasing SOC amendment elevated elemental concentrations in leachate for all elements except Al. In addition, we observe a negative SOC x basalt interaction effect for Fe ($p=0.05$), K ($p=0.03$) and a non-significant interaction tendency for TA leaching ($p=0.11$). Although not significant, this tendency for a negative SOC x basalt interaction can be observed also for all other elements in **Figure 2** (except for Al).

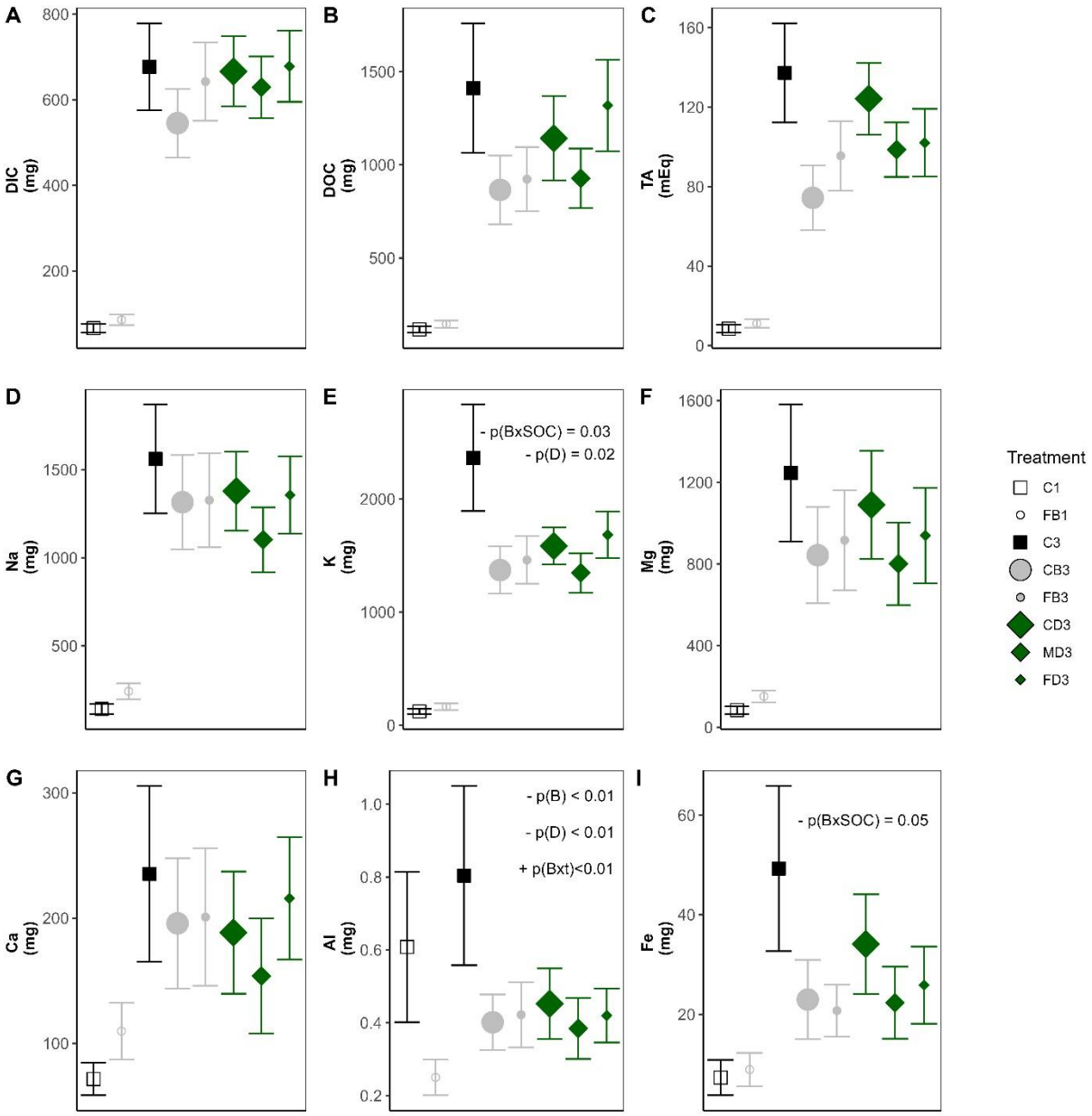

278

279 **Figure 2:** Leachate mass (in mg for elements and mEq for TA) of (A) DIC (B) DOC (C) TA (D)
280 Na (E) K (F) Mg (G) Ca (H) Al and (I) Fe flushed from the soil, combining all leachate data from
281 days 14, 56, and 113 after amendment. Points and error bars indicate averages from all leachate
282 samplings ± standard errors of the mean. Raw data of every separate leachate collection is shown
283 in in Fig.S2 and Fig. S3. Green, grey and black symbols are dunite, basalt and controls,
284 respectively. 1% and 3% SOC soils are unfilled and filled respectively; The size of the symbols
285 reflects the particle size of the rocks. Significant effects are indicated as p(B) for basalt
286 amendment, p(D) for dunite, p(BxSOC) for basalt x SOC interaction and p(B size) and p(D size)
287 for t basalt and dunite size effects, respectively. Extended leachate data for all leaching dates can
288 be found in **Fig. S2** and **Fig. S3.** Significant effects are indicated in this figure , an extended

overview of statistics can be found in **Table S2**. For Al, the basalt effect was negative and $p<0.01$ for both of the two subsets of the dataset.

3.1.2 Soil inorganic C

No significant changes in bulk soil SIC were found after basalt/dunite amendment (**Table 5**). Not only in the bulk soil, but also in mesh bags filled with pure silicates we did not observe accumulation of carbonates. In mesh bags filled with dunite, SIC was even lower after 119 days relative to the start of the experiment, when finer dunite was applied ($p<0.01$, **Fig. S4)**.

Only treatment FB1 showed an increase in ΔSIC (~0.1 t C ha^{-1}). FB1 (1% SOC with basalt) was also the only treatment in which PHREEQCENTURY predicted higher SIC than the control (**Figure 3**). The model suggested that Ca from basalt weathering formed Ca-montmorillonite rather than $CaCO_3$, while predictions indicate that Mg preferentially formed chlorite instead of Mg-carbonates. PHREEQCENTURY overestimated ΔSIC in FB1, but this was reduced by raising the $CaCO_3$ saturation index threshold from 0 to 1. Manure alone significantly increased SIC (Table 5), but no significant basalt × SOC interaction was detected.

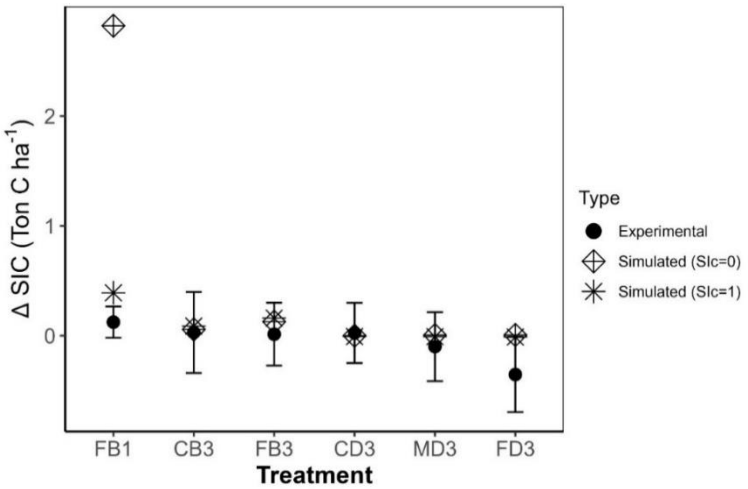

Figure 3: Comparison of simulated and experimental SIC change after 130 days, calculated from carbonate-associated base cations as in **Equation 1**. Dots and error bars show experimental averages and standard errors of the mean for SIC, quantified from base cations in soil extracts

leached with acetate. Simulations were repeated for two different carbonate precipitation thresholds (SIc=0 or SIc=1).

Table 5: Summary statistics for dissolved inorganic carbon (DIC) in leachates, soil inorganic carbon (SIC) (after 130 days) and cumulative soil CO_2 efflux (SCE) after 389 days. Effects of each predictor on the response variable are expressed as regression coefficients, with corresponding p-values in parentheses. For the SOC × basalt and time x basalt interaction, p-values are only shown when significant; non-significant interaction terms were removed from the final model (indicated with N.S.). "/" is written for time effects in measurements that were not repeated in time.

	Treatments in dataset: C3, FB3, CB3, FD3, MD3, CD3					**Treatments in dataset: C1, FB1, C3, FB3**			
y-variable (Unit)	**Basalt effect**	**Particle size basalt**	**Basalt x time**	**Dunite effect**	**Particle size Dunite**	**Basalt effect**	**SOC**	**Basalt x SOC**	**Basalt x time**
DIC (mg) (389 days)	+40.18 (0.97)	-0.26 (0.41)	N.S.	-21.6 (0.98)	0 (0.97)	-6.12 (0.93)	**290.92 (<0.01)**	N.S.	N.S.
SIC (%) (130 days)	+10 e -5 (p=1.00)	2e-6 (p=0.96)	/	-0.019 (p=0.29)	2e-5 (p=0.23)	+0.005 (p=0.60)	**+0.040 (p<0.01)**	N.S.	/
Cumulative SCE (ton C/ha) (389 days)	-0.15 (p=0.99)	+0.01 (p=0.37)	/	-2.79 (p=0.59)	+6 e-3 (p=0.22)	+1.24 (p=0.66)	**+10.98 (p<0.01)**	N.S.	/

3.2 Sequential extractions

The sequential extractions revealed that rock amendments redistributed Fe, Al and base cations among different soil pools (**Figure 4; Table 6**). Basalt amendment significantly increased exchangeable Ca and Al (**Table 6**). In the carbonate pool, the only significant change was a decrease in Fe with basalt addition. The reducible pool showed a relatively large and significant Mg increase after basalt and dunite amendment. Basalt also significantly increased oxidizable (SOM-associated) Mg, Al and Ca and dunite increased oxidizable Mg (**Figure 4**, **Table 6**). Rock particle size did not significantly affect elements in the extracted soil pools.

Amendment with only organics significantly increased all elements throughout all Tessier-extractable soil pools, except for exchangeable Fe and Al, reducible Mg and oxidizable K. In addition, we observed negative interaction effects between SOC and basalt: exchangeable Ca (**Figure 4C**) and reducible Mg (**Figure 4D**) significantly decreased in basalt-amended soils at higher SOC (both p=0.01). The sum of elements recovered from all extracted soil pools can be compared with the weathered element fluxes predicted by PHREEQCENTURY. As shown in **Figure 4**, the magnitude of the observed increase in soil weathering products is broadly consistent with PHREEQC predictions, which reproduced the correct order of magnitude of weathering products using weathering rates from Palandri et al. (2004) (after 130 days of experiment).

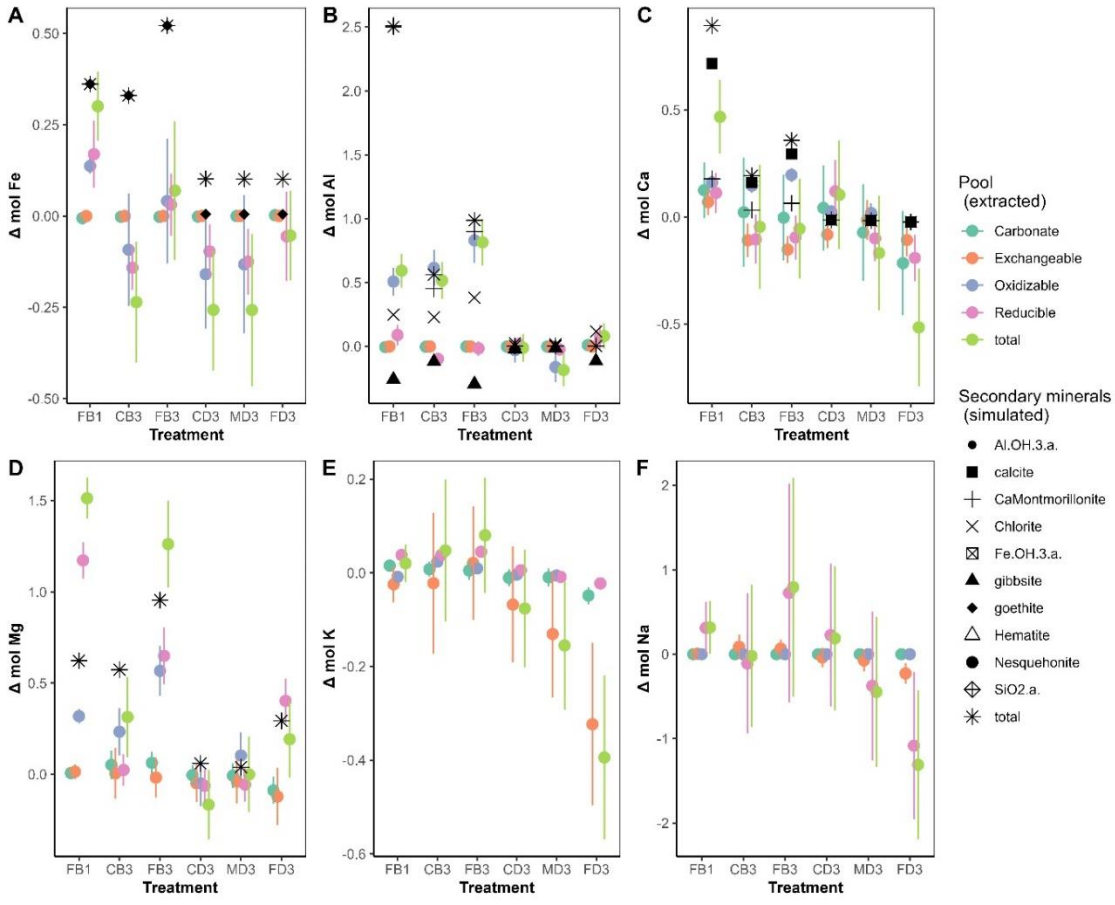

Figure 4: Changes in elemental concentrations in the extracted soil pools (Tessier extractions, colored symbols) after 130 days, for each treatment relative to control soils and comparison with simulated secondary minerals for (A) Fe, (B) Al, (C) Ca, (D) Mg, (E) K and (F) Na. Only those secondary minerals are shown that were formed according to the model. Colored symbols and error bars show experimental averages and standard errors of the mean. No Na- and K-bearing secondary minerals were allowed to form in simulations. Results of the statistical analyses are provided in **Table 6.** Symbols for totals for Mg overlap with Chlorite, while the total increase in Fe-bearing secondary minerals in basalt and dunite soils overlap with goethite and hematite respectively. A saturation index threshold for carbonate formation of 1 was used in these simulations. Note that for dunite, the visualized increase in Fe-holding secondary minerals is a consequence of the amendment with hematite rather than neoformation of Fe-holding secondary minerals.

Table 6: Results of the statistical analyses for the treatment effects (SOC, basalt, basalt particle size, dunite particle size and dunite) on the Tessier sequential extraction fractions for different soil pools and elements**.** Soil samples for these measurements were taken after 130 days. Effect estimates coefficients are presented with corresponding p-values in (parentheses). For the SOC × basalt interaction, p-values are only shown when significant; non-significant interaction terms were removed from the final model (indicated with N.S.).

		Treatments in dataset: C3, FB3, CB3, FD3, MD3, CD3				**Treatments in dataset: C1, FB1, C3, FB3**		
pool	**element**	**Basalt**	**Basalt particle size**	**Dunite**	**Dunite particle size**	**Basalt**	**SOC**	**Basalt x SOC**
Exchangeable	Fe	**-2.3e-04 (0.04)**	3.4e-07 (0.06)	-3e-05 (0.65)	**1.3e-07 (0.05)**	**-2.4e-04 (0.03)**	-4.8e-05 (0.34)	N.S.
Exchangeable	Al	3.7e-03 (0.41)	-2.8e-06 (0.7)	4.5e-03 (0.11)	-5.1e-07 (0.85)	**4.7e-03 (0.03)**	4.7e-04 (0.63)	N.S.
Exchangeable	Ca	-1.9e-01 (0.09)	1.1e-04 (0.52)	-6.6e-02 (0.33)	-4.9e-06 (0.94)	**1.8e-01 (0.05)**	**1.6e-01 (<0.01)**	**-1.1e-01 (0.01)**
Exchangeable	Mg	-3.5e-02 (0.84)	6.1e-05 (0.84)	-9.5e-02 (0.41)	5.3e-05 (0.64)	-5.8e-04 (0.99)	**2.8e-01 (<0.01)**	N.S.
Exchangeable	K	5.4e-02 (0.79)	-1.1e-04 (0.73)	**-2.7e-01 (0.04)**	2.2e-04 (0.09)	-3.1e-03 (0.95)	**4.2e-01 (<0.01)**	N.S.
Exchangeable	Na	5.2e-02 (0.73)	5.5e-05 (0.82)	-1.8e-01 (0.06)	1.6e-04 (0.1)	3.4e-02 (0.43)	**2.3e-01 (<0.01)**	N.S.
Carbonate	Fe	-3e-03 (0.44)	1.2e-06 (0.85)	1.8e-03 (0.46)	-3.4e-06 (0.17)	**-4.3e-03 (0.01)**	**-8.5e-03 (<0.01)**	N.S.
Carbonate	Al	1.9e-04 (0.99)	-3.9e-06 (0.83)	7e-03 (0.32)	-9e-06 (0.2)	-2.9e-03 (0.56)	**-2.3e-02 (<0.01)**	N.S.

pool	element	Treatments in dataset: C3, FB3, CB3, FD3, MD3, CD3				Treatments in dataset: C1, FB1, C3, FB3		
		Basalt	**Basalt particle size**	**Dunite**	**Dunite particle size**	**Basalt**	**SOC**	**Basalt x SOC**
Carbonate	Ca	-2.3e-02 (0.94)	6.7e-05 (0.9)	-1.9e-01 (0.33)	2.4e-04 (0.23)	6.4e-02 (0.56)	**4.1e-01 (<0.01)**	N.S.
Carbonate	Mg	7.1e-02 (0.45)	-2.9e-05 (0.85)	-6.3e-02 (0.3)	6.5e-05 (0.28)	3.3e-02 (0.21)	**1.5e-01 (<0.01)**	N.S.
Carbonate	K	2.8e-03 (0.92)	7.5e-06 (0.88)	-3.6e-02 (0.06)	2.9e-05 (0.12)	1e-02 (0.25)	**4.7e-02 (<0.01)**	N.S.
Reducible	Fe	1.6e-01 (0.29)	-4.6e-04 (0.08)	-8.3e-02 (0.4)	-2.1e-05 (0.82)	1e-01 (0.12)	**-1.4e-01 (<0.01)**	N.S.
Reducible	Al	4.8e-02 (0.67)	-2.2e-04 (0.26)	3.4e-02 (0.64)	-2.5e-05 (0.72)	4e-02 (0.41)	**-1.7e-01 (<0.01)**	N.S.
Reducible	Ca	-8.8e-02 (0.57)	-2.5e-05 (0.92)	**-2e-01 (0.05)**	3.2e-04 (<0.01)	1.4e-02 (0.83)	**1.2e-01 (<0.01)**	N.S.
Reducible	Mg	**1.1e+00 (<0.01)**	**-1.7e-03 (<0.01)**	**2.6e-01 (0.06)**	**-3.6e-04 (0.01)**	**1.4e+00 (<0.01)**	1e-01 (0.14)	**-2.6e-01 (0.01)**
Reducible	K	**5e-02 (<0.01)**	-1.8e-05 (0.37)	**-2.1e-02 (0.01)**	**2.7e-05 (<0.01)**	**4.1e-02 (<0.01)**	**1.6e-02 (<0.01)**	N.S.
Reducible	Na	1.4e+00 (0.26)	-2.2e-03 (0.27)	-9.7e-01 (0.21)	1.2e-03 (0.11)	5.1e-01 (0.43)	**1.1e+00 (<0.01)**	N.S.
Oxidizable	Fe	1.4e-01 (0.53)	-3.5e-04 (0.36)	-1.2e-01 (0.51)	-3.6e-05 (0.85)	9.2e-02 (0.25)	**3.1e-01 (<0.01)**	N.S.
Oxidizable	Al	**1e+00 (<0.01)**	-5.7e-04 (0.12)	-2.1e-01 (0.23)	1.8e-04 (0.34)	**6.6e-01 (<0.01)**	**3.9e-01 (<0.01)**	N.S.
Oxidizable	Ca	**2.3e-01 (<0.01)**	-1.3e-04 (0.17)	1.6e-02 (0.72)	7.8e-06 (0.87)	**1.8e-01 (<0.01)**	**3.4e-02 (<0.01)**	N.S.
Oxidizable	Mg	**8.3e-01 (<0.01)**	**-8.8e-04 (<0.01)**	1.6e-01 (0.13)	-2e-04 (0.07)	**4.4e-01 (<0.01)**	**1.5e-01 (<0.01)**	N.S.
Oxidizable	K	-1.7e-03 (0.85)	**3.8e-05 (0.02)**	-6.8e-03 (0.36)	3.3e-06 (0.67)	-9.6e-05 (0.98)	4.3e-03 (0.08)	N.S.

356

357 3.3 **Changes in SSA**

358 In general, BET-SSA was larger for finer particles, with the exception of coarse dunite, which had
359 a larger BET-SSA than medium dunite (CD3 versus MD3). BET-SSA was not constant in time as
360 basalts' BET-SSA decreased in soils with higher SOC: BET-SSA of FB3 decreased with
361 approximately 2 units more than the BET-SSA of FB1 (**Figure 5**). The BET-SSA change in time
362 was significantly more negative for basalt than for dunite treatments ($p<0.01$).

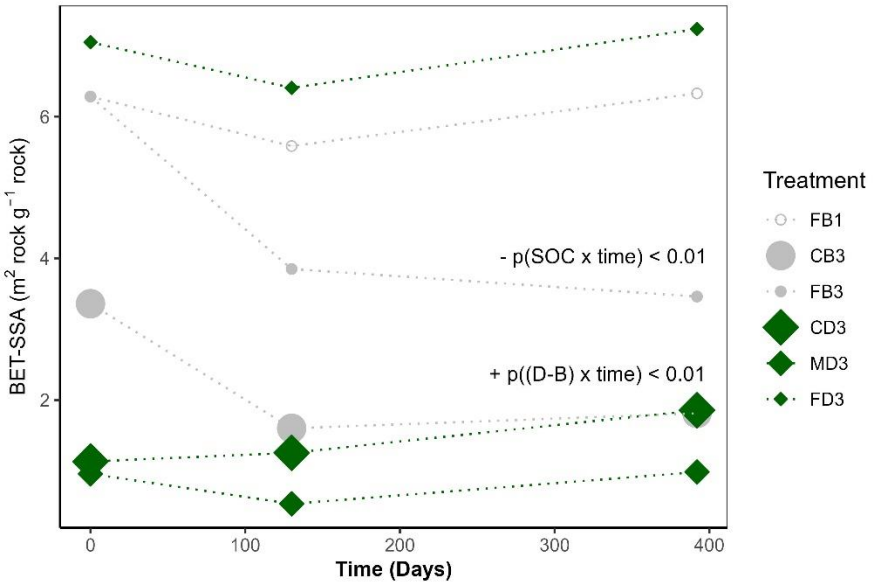

363

364 **Figure 5:** Temporal evolution of BET-SSA. n=3 for day 0 and day 130, n=1 for day 389, note that
365 plotted points are larger than error bars and that the standard error of the mean is not visible in this
366 figure. The positive D-B x time effect means that the BET-SSA change in time was significantly
367 more positive for dunite than for basalt.

368 **3.4 SCE**

369 The SCE showed strong temporal variation, which was partly associated with changes in
370 temperature (Figure S9). We did not observe any significant treatment effect on SCE dynamics
371 (**Table 6)** or on cumulative SCE after 389 days (**Table 5).**

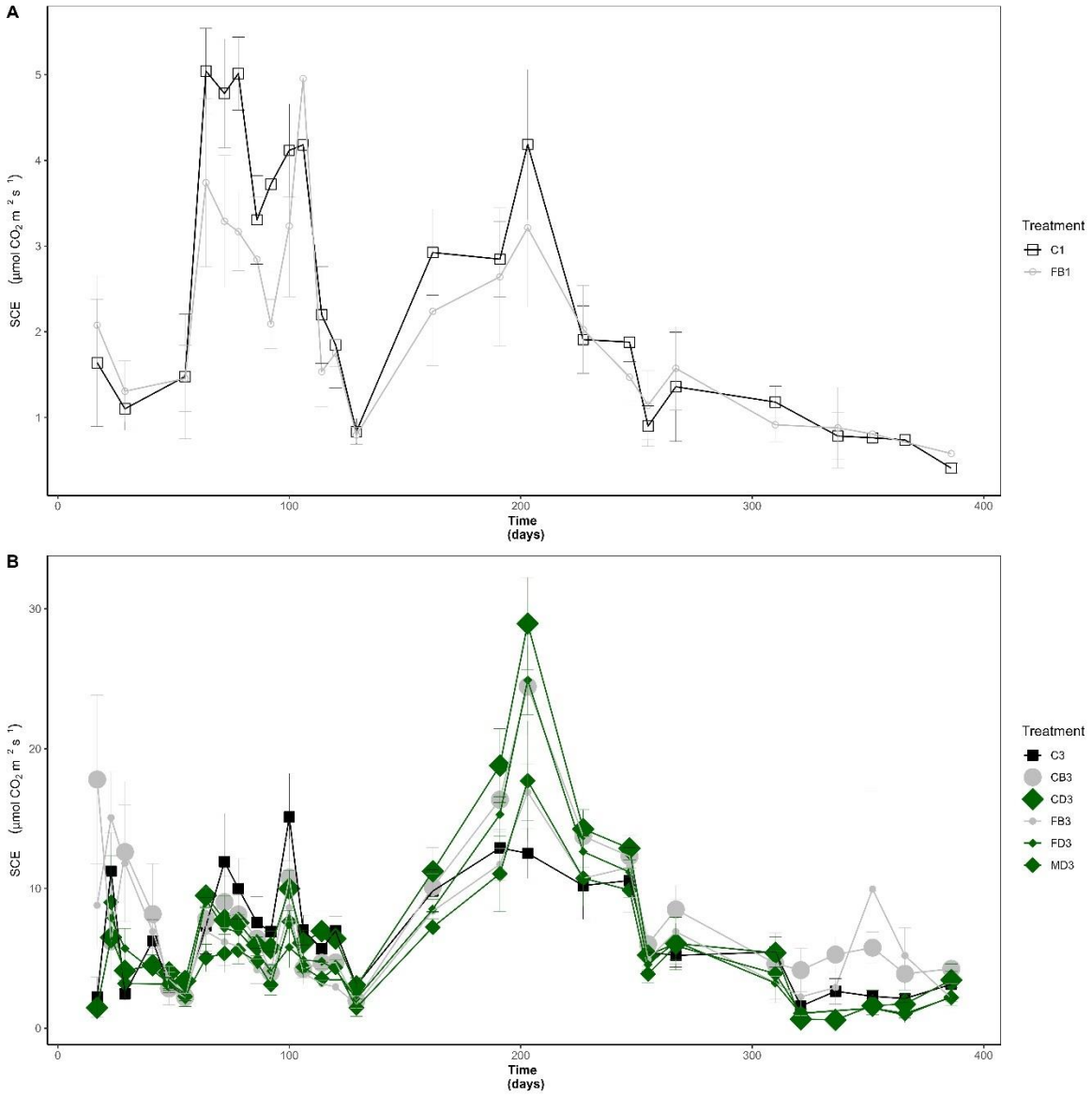

Figure 6: Difference in soil CO_2 efflux (µmol CO_2 m^{-2} s^{-1}) over time for treatments (A) 1% SOC soils and (B) 3% SOC soils.

Table 6: Effects of parameters (basalt, SOC, SOC x basalt interaction, dunite amendment, basalt and dunite d90 particle size) on SCE residuals (in µmol/m²/s), with p values in parentheses. Significant values are indicated in bold. For the SOC × basalt interaction, p-values are only shown when significant; non-significant interaction terms were removed from the final model (indicated with N.S.).

Treatments in dataset: C3, FB3, CB3, FD3, MD3, CD3						Treatments in dataset: C1, FB1, C3, FB3			
Basalt	**Basalt particle size**	**Basalt x Time**	**Dunite**	**Dunite particle size**	**Dunite x Time**	**Basalt**	**Basalt x Time**	**SOC**	**SOC x Basalt**
-0.36 (0.90)	0.10e-2 (0.72)	N.S.	-0.30 (0.85)	0.54e-3 (0.53)	N.S.	-0.11 (0.78)	N.S.	0.34 (0.09)	N.S.

4. Discussion

4.1 Inhibition of inorganic CO_2 removal

Contrary to our expectations, silicate amendments did not significantly increase DIC (**Table 5**). This is in line with several other EW studies that failed to detect significant DIC increases in leachates from basalt and dunite amended soils (Amann et al., 2020; Holden et al., 2024; Steinwidder et al., 2025), despite weathering being evident from base cation monitoring.

Besides the absence of a DIC increase, we did not observe significant accumulation of soil inorganic carbon (SIC). Although carbonates were oversaturated in our simulations, the model predicted no (for dunite) to modest pedogenic carbonate formation (for treatment FB1) (**Figure 3**), even in this alkaline soil-manure mixture (soil pH was approximately 8, see **Fig S3.D**). The absence of significant SIC accumulation is in contrast with basalt quarry fine amendment where a substantial SIC increase (up to 30% SIC) was detected after 7 years (Manning et al., 2013). Notably, Manning et al. (2013) applied a substantial rate (about 7,500 t ha^{-1}, corresponding to a 25 cm layer of basalt with an assumed density of 3 g cm^{-3}). Lei et al., (2025) only applied 50 t basalt ha^{-1} and observed a small increase in SIC (0.5-1 mg g^{-1} soil). In another, three year duration, agricultural field study, SIC was increased significantly (yet <0.5 mg g^{-1} soil) after basalt addition (and only without compost and/or biochar co-amendment; Sohng et al., 2025).

Together, these studies indicate that basalt amendments generally result in only small SIC increases (<1 mg/g soil), consistent with our findings. In our experiment, the treatment with the highest SIC increase was the 1% SOC soil. Here, the addition of 100 t basalt ha^{-1} increased SIC by 0.45 ± 0.52 t CO_2 ha^{-1} after 130 days, which is equivalent to a sequestration of 0.013 ± 0.015 t CO_2 t^{-1} basalt $year^{-1}$. This increase was thus minor, and not statistically significant, indicating very limited realized CDR.

Hydrological conditions may have contributed to the low CDR realization in our experiment. The irrigation flux was relatively low (223 mm yr^{-1}), with only ~23% infiltrating due to evaporation - conditions that likely favored secondary mineral formation. While relatively low, this flux is comparable to dryland agriculture, whereas tropical soils with more rainfall may export more DIC. However, recent field studies in both temperate and tropical regions report similarly low CDR based on DIC export, with estimates of ~0.0001–0.001 t CO_2 t^{-1} basalt y^{-1} (Anthony et al., 2025; Holden et al., 2024; Mcbride et al., 2025), which is two to three orders of magnitude below inorganic CO_2 removal estimates used for upscaling by for example Beerling et al. (2020). More recent commercial EW field trials by InPlanet in Brazil, using lower basalt application rates (10-20 t ha^{-1}) are more encouraging (0.038-0.064 t gross CDR t^{-1} basalt $year^{-1}$ and 0.025-0.036 t net CDR t^{-1} basalt $year^{-1}$, after deduction of life cycle emissions; Isometric, 2025)), yet still one order of magnitude lower than the ~ 0.154 t CO_2 t^{-1} basalt y^{-1} assumed by Beerling et al. (2020).

Low DIC export and low inorganic CDR do not necessarily reflect low weathering rates. Rock weathering can proceed without DIC export when base cations released during dissolution are retained in soils. Cation retention can occur through cation exchange, sorption processes and uptake in clays, all of which generate acidity that promotes CO_2 degassing rather and suppress carbonate formation and leaching. Capturing this behavior in EW models therefore requires

representing these cation-scavenging mechanisms explicitly. Currently, EW is commonly modelled by applying empirical reduction factors to intrinsic mineral dissolution rates (Bertagni et al., 2024). In contrast, our mechanistic approach uses dissolution kinetic constants from existing databases (Palandri et al., 2004) and regulates inorganic CO_2 removal through modelling base cation scavenging in soils (**Figure 4**).

Although our model and data suggest substantial base-cation scavenging, uncertainty remains regarding the mineral phases responsible for base cation retention. According to model predictions, base cation-bearing clay minerals (such as montmorillonite and chlorite) formed preferentially over $CaCO_3$ and $MgCO_3.H_2O$ (**Figure 4**), producing protons and shifting the system towards CO_2 degassing. Clays were not allowed to form in several previous EW modelling (Kelland et al., 2020), which instead directed base cations exclusively to carbonate formation. Our results suggest that inorganic CDR may have been overestimated in these models by Kelland et al. (2020) and Vienne et al., (2022). Although clay formation was suggested earlier in the context of EW (Iff et al., 2024; Vienne et al., 2024) (Iff et al., 2024; Steinwidder et al., 2026; Vienne et al., 2024) and is quantifiable with Li isotopes (Pogge von Strandmann et al., 2021, 2022, 2025), clay formation is challenging to quantify and remains uncertain based on our dataset. If no base cation bearing clays would be formed here, the acidity release may have been entirely due to cation sorption to amorphous (hydr)oxides and SOM.

Co-amending rocks with organic matter was expected to enhance weathering rates while suppressing secondary clay mineral and pedogenic carbonate formation through CO_2-driven pH lowering. However, we found no indications that higher SOC stimulated weathering rates, as none of the weathering indicators (DIC and TA leaching, SIC formation, as well as base cations in the different soil fractions) increased for the high SOC basalt treatment (**Figure 2-4**). We speculate

that increased acidity release from organic matter decomposition and organic acids promoted degassing of CO_2, outweighing the expected positive effect of higher CO_2 pressure and reduced secondary mineral formation on the weathering rates. Accordingly, Lei et al. (2025) observed SIC increases after basalt addition only without organic (straw) amendment, as straw-derived acids lowered pH, reducing DIC and SIC.

The lack of increased SIC formation and DIC leaching with higher amendments may result not only from acidity release but also from surface passivation inhibiting primary mineral weathering. The formation of inert, 'unweatherable' coatings could passivate rock surfaces and prevent rock weathering (Amann et al., 2020). Inhibitory surface coatings that can reduce olivine weathering by an order of magnitude are known to be amorphous SiO_2 and $Fe(OH)_3$ (Oelkers et al., 2018), yet also organic passivation coatings could slow down weathering (Corbett et al., (2024).

In our experiment, basalt BET-SSA declined with higher SOC, pointing to the formation of surface coatings that may have reduced mineral reactivity and thus inorganic CO_2 removal. Potentially, a combination of the abovementioned compounds (clays, Fe-hydroxides) crosslinked with DOC, creating a 'organo-minerallic glue' or mineral associated organic matter (MAOM) (Heckman et al., 2018; Wagai et al., 2013). Sequential "Heckman" extractions showed declining Al and Si weathering between day 130 and 389 (**Fig. S5, S6 and S7**), with Mg, Ca, and Fe even decreasing (suggesting incorporation into more crystalline or organo-mineral forms resistant to extraction). These findings, consistent with Steinwidder et al. (2025), indicate that newly formed (organo)minerals contributed to surface passivation and reduced inorganic CO_2 removal in our experiment.

4.2 SOM responses to EW and implications for modeling

SOM may not only influence inorganic CO_2 removal, the decomposition of SOM itself can also be influenced by rock amendment. Rock weathering can influence decomposition of SOM in multiple ways, including through changes in pH, moisture and DOC sorption to secondary minerals.

Soil water pH, measured at atmospheric pCO_2, exceeded 8 in all treatments (likely due to $CaCO_3$ in the input manure). At higher pCO_2 conditions in soils, model simulations predicted a pH of pH 7 in 3% SOC soils while 1% SOC soils had a relatively lower pCO_2 so that pH remained above 8. Nonetheless, this shift had little effect on decomposition and could not explain SCE patterns, pointing to other drivers such as moisture or temperature. According to the Gompertz relationship, soil moisture was non-limiting (normalized SWC >0.2 in all treatments; Sierra et al., 2015). Hence, the moisture modifier remained 1 in all treatments. Despite the significant increase in SWC after basalt amendment (**Fig. S1**), the model thus did not predict differences in decomposition from moisture changes (**Fig. S10**), unlike in other models (Demeter, Standcarb) that also account for excess-moisture inhibition of decomposition.

While our modelling results indicate that rock amendments had only minor effects on SOM decomposition, we also found indications for effects on SOC stabilization. The model predicted that Fe and Al release can positively impact SOC through MAOM formation, although the magnitude was small (~100 kg MAOM-C ha^{-1} in 3% SOC basalt mesocosms (**Fig. S11**) and even less MAOM-C in dunite soils). In addition, clays influenced the distribution between active and slow SOM pools (**Fig. S11**). Nonetheless, PHREEQCENTURY's prediction for MAOM-C remain uncertain because MAOM-C cannot be directly measured or compared with observational data.

To disentangle contributions of SOM stabilization in the form of MAOM and decomposition of labile SOC pools (e.g. particulate organic matter (POM)), models with well defined, measurable

MAOM pools are needed. The MEMS framework addresses this need by representing 14 measurable soil C pools where POM, MAOM, and litter chemistry jointly govern SOM dynamics (Zhang et al., 2021). Although MEMS represents the current SOM paradigm well, its large number of pools complicates parameterization, and it omits key factors such as pH effects on decomposition and SOM stabilization through aggregation. Aggregates should be included in coupled EW–SOC models, as enhanced SOM occlusion has been observed in EW studies (Sokol et al., 2024; Steinwidder et al., 2025). To the best of our knowledge, only the Millennial model has achieved simulation of aggregate formation (Abramoff et al., 2018), with inclusion of a pH modifier using a lower amount of measurable pools relative to MEMS (Abramoff et al., 2022). Hence, Millennial may serve as a suitable alternative to the CENTURY model for developing future integrated EW–SOC models.

5. Conclusion

In this study, we did not observe significant inorganic CO_2 removal after soil amendment with basalt and dunite, despite clear weathering signals. Base cations were retained in soil pools associated with hydroxides and SOM, preventing DIC leaching, with only modest SIC formation. Base cation scavenging by exchange, and sorption to (hydr)oxides and SOM generated acidity that counteracted inorganic CO_2 removal. PHREEQCENTURY simulations indicated that dissolved base cations preferentially precipitated into secondary clays rather than pedogenic carbonates, reducing inorganic CDR.

While we expected that higher CO_2 production in organic-rich soils would stimulate realized inorganic CO_2 removal, we did not observe a stimulation in DIC efflux and SIC did not increase in amended 3% SOC soils. Basalt specific surface area decreased in the presence of more SOC, indicating inhibitory surface passivation of SOC for weathering.

These findings suggest that the fraction of inorganic CO_2 removal realized in the field will depend on SOC inputs and mineralogical context, and may be substantially lower than implied by approaches that neglect cation scavenging and secondary mineral formation. Improving field-scale predictions will require integrating mechanistic mineral and SOC controls into EW models and validating these processes across contrasting soils, climates and management regimes.

Supporting Information.

All supplementary Tables and Figures can be found in the file 'SI.docx'. The model code and required model functions can be found in the zipfile 'modelcode.zip. Experimental data and R scripts are made publicly available in zenodo: https://zenodo.org/records/18018582.

AUTHOR INFORMATION

Author Contributions

The manuscript was written through contributions of all authors. All authors have given approval to the final version of the manuscript. Contribution by author: TC: implementation of the coupled model in R studio, HN: co-executed experiment during intensive monitoring phase (first 130 days). BG: implementation Centruy model. CV: drafted discussion on SOM models and the requirement for measurable pools. Heckman extractions were executed in collaboration with LS. RP: executed the BET-SSA measurements. SV: research conceptualization, assistance in writing and general supervision.

Funding Sources

We also acknowledge support of the UPSURGE project, which has received funding from the European Union's Horizon 2020 research and innovation program under grant agreement No 101003818. This research was supported by the Research Foundation— Flanders (FWO) [1S06325N], 1174925N] and [G000821N] (Biotic controls of the potential of enhanced silicate weathering for land-based climate change mitigation) and the C-Farms project (S004023N). BG received government funding from the ALAMOD project of the exploratory research program FairCarboN managed by the Agence Nationale de la Recherche under the France 2030 program (ANR-22-PEXF-002-projet ALAMOD).

ACKNOWLEDGMENTS

We thank Anne Cools, Steven Joosen and Anke De Boeck for their assistance with ICP-OES for sequential extraction samples. A large language model (Microsoft Copilot) was utilized to enhance the clarity, grammar, and phrasing of language in this manuscript.

ABBREVIATIONS

CDR, Carbon dioxide removal, DIC, dissolved inorganic C; DOC, dissolved organic C; EW, Enhanced Weathering; MAOM, Mineral-associated organic matter; POM, Particulate organic matter; RTM Reactive transport model; SI, Saturation index; SIC, Soil inorganic Carbon; SOC, Soil organic Carbon; SOM, Soil organic Matter; t , ton.

REFERENCES

Abramoff, R., Xu, X., Hartman, M., O'Brien, S., Feng, W., Davidson, E., Finzi, A., Moorhead, D., Schimel, J., Torn, M., & Mayes, M. A. (2018). The Millennial model: in search of measurable pools and transformations for modeling soil carbon in the new century. *Biogeochemistry*, *137*(1–2), 51–71. https://doi.org/10.1007/s10533-017-0409-7

Abramoff, R. Z., Guenet, B., Zhang, H., Georgiou, K., Xu, X., Viscarra Rossel, R. A., Yuan, W., & Ciais, P. (2022). Improved global-scale predictions of soil carbon stocks with Millennial Version 2. *Soil Biology and Biochemistry*, *164*(May 2021), 108466. https://doi.org/10.1016/j.soilbio.2021.108466

Amann, T., Hartmann, J., Hellmann, R., Pedrosa, E. T., & Malik, A. (2022). Enhanced weathering potentials—the role of in situ CO2 and grain size distribution. *Frontiers in Climate*, *4*. https://doi.org/10.3389/fclim.2022.929268

Amann, T., Hartmann, J., Struyf, E., De Oliveira Garcia, W., Fischer, E. K., Janssens, I., Meire, P., & Schoelynck, J. (2020). Enhanced Weathering and related element fluxes - A cropland mesocosm approach. *Biogeosciences*, *17*(1), 103–119. https://doi.org/10.5194/bg-17-103-2020

Anthony, T. L., Jones, A. R., & Silver, W. L. (2025). Supplementing Enhanced Weathering With Organic Amendments Accelerates the Net Climate Benefit of Soil Amendments in Rangeland Soils. *AGU Advances*, *6*(2). https://doi.org/10.1029/2024AV001480

Beerling, D. J., Kantzas, E. P., Lomas, M. R., Wade, P., Eufrasio, R. M., Renforth, P., Sarkar, B., Andrews, M. G., James, R. H., Pearce, C. R., Mercure, J. F., Pollitt, H., Holden, P. B., Edwards, N. R., Khanna, M., Koh, L., Quegan, S., Pidgeon, N. F., Janssens, I. A., … Banwart, S. A. (2020). Potential for large-scale CO2 removal via enhanced rock weathering with croplands. *Nature*, *583*(7815), 242–248. https://doi.org/10.1038/s41586-020-2448-9

Bertagni, M. B., Calabrese, S., Cipolla, G., Valerio Noto, L., & Porporato, A. M. (2024). Advancing Enhanced Weathering Modeling in Soils: Systematic Comparison and Validation with Experimental Data. *Journal of Advances in Modeling Earth Systems*, 1–25. https://doi.org/10.22541/essoar.170559500.09183720/v1

Boito, L., Steinwidder, L., Rijnders, J., Berwouts, J., Janse, S., Niron, H., Roussard, J., Vienne, A., & Vicca, S. (2025). Enhanced Rock Weathering Altered Soil Organic Carbon Fluxes in a Plant Trial. *Global Change Biology*, *31*(8), 1–19. https://doi.org/10.1111/gcb.70373

Camino-Serrano, M., Guenet, B., Luyssaert, S., Ciais, P., Bastrikov, V., De Vos, B., Gielen, B., Gleixner, G., Jornet-Puig, A., Kaiser, K., Kothawala, D., Lauerwald, R., Peñuelas, J., Schrumpf, M., Vicca, S., Vuichard, N., Walmsley, D., & Janssens, I. A. (2018). ORCHIDEE-SOM: Modeling soil organic carbon (SOC) and dissolved organic carbon (DOC) dynamics along vertical soil profiles in Europe.

578 *Geoscientific Model Development*, *11*(3), 937–957. https://doi.org/10.5194/gmd-11-937-2018

579 Corbett, T. D. W., Westholm, M., Rosling, A., Calogiuri, T., Poetra, R., Niron, H., Hagens, M., Vidal, A., Van
580 Groenigen, J. W., Hartmann, J., Janssens, I. A., Rieder, L., Struyf, E., Van Tendeloo, M., Vlaeminck, S.
581 E., Vicca, S., & Neubeck, A. (2024). Organic carbon source controlled microbial olivine dissolution in
582 small-scale flow-through bioreactors, for CO2 removal. *Npj Materials Degradation*, *8*(1).
583 https://doi.org/10.1038/s41529-024-00454-w

584 Dimassi, B., Guenet, B., Saby, N. P. A., Munoz, F., Bardy, M., Millet, F., & Martin, M. P. (2018). The impacts
585 of CENTURY model initialization scenarios on soil organic carbon dynamics simulation in French long-
586 term experiments. *Geoderma*, *311*(October 2017), 25–36.
587 https://doi.org/10.1016/j.geoderma.2017.09.038

588 Heckman, K., Lawrence, C. R., & Harden, J. W. (2018). A sequential selective dissolution method to
589 quantify storage and stability of organic carbon associated with Al and Fe hydroxide phases.
590 *Geoderma*, *312*(September 2017), 24–35. https://doi.org/10.1016/j.geoderma.2017.09.043

591 Hellmann, R., Daval, D., & Wirth, R. (2013). Formation of Amorphous Silica Surface Layers by Dissolution-
592 Reprecipitaton During Chemical Weathering: Implications for CO2 Uptake. *Procedia Earth and*
593 *Planetary Science*, *7*(May), 346–349. https://doi.org/10.1016/j.proeps.2013.03.154

594 Holden, F. J., Davies, K., Bird, M. I., Hume, R., Green, H., Beerling, D. J., & Nelson, P. N. (2024). In-field
595 carbon dioxide removal via weathering of crushed basalt applied to acidic tropical agricultural soil.
596 *Science of the Total Environment*, *955*(October), 176568.
597 https://doi.org/10.1016/j.scitotenv.2024.176568

598 Iff, N., Renforth, P., & Pogge von Strandmann, P. A. E. (2024). The dissolution of olivine added to soil at
599 32°C: the fate of weathering products and its implications for enhanced weathering at different
600 temperatures. *Frontiers in Climate*, *6*(April), 1–18. https://doi.org/10.3389/fclim.2024.1252210

601 IPCC. (2023). Summary for Policymakers of the Intergovernmental Panel on Climate Change. *Climate*
602 *Change 2023: Synthesis Report. Contribution of Working Groups I, II and III to the Sixth Assessment*
603 *Report of the Intergovernmental Panel on Climate Change*, *pp. 1-34*.
604 https://doi.org/10.59327/IPCC/AR6-9789291691647.001

605 Isometric. (2025). *Isometric registry*. https://registry.isometric.com/

606 Kelland, M. E., Wade, P. W., Lewis, A. L., Taylor, L. L., Sarkar, B., Andrews, M. G., Lomas, M. R., Cotton, T.
607 E. A., Kemp, S. J., James, R. H., Pearce, C. R., Hartley, S. E., Hodson, M. E., Leake, J. R., Banwart, S. A.,
608 & Beerling, D. J. (2020). Increased yield and CO2 sequestration potential with the C4 cereal Sorghum
609 bicolor cultivated in basaltic rock dust-amended agricultural soil. *Global Change Biology*, *26*(6),
610 3658–3676. https://doi.org/10.1111/gcb.15089

611 Klemme, A., Rixen, T., Müller, M., Notholt, J., & Warneke, T. (2022). Destabilization of carbon in tropical
612 peatlands by enhanced weathering. *Communications Earth and Environment*, *3*(1), 1–9.
613 https://doi.org/10.1038/s43247-022-00544-0

614 Knapp, W. J., & Tipper, E. T. (2022). The efficacy of enhancing carbonate weathering for carbon dioxide
615 sequestration. *Frontiers in Climate*, *4*. https://doi.org/10.3389/fclim.2022.928215

616 Kothawala, D. N., Moore, T. R., & Hendershot, W. H. (2009). Soil Properties Controlling the Adsorption of
617 Dissolved Organic Carbon to Mineral Soils. *Soil Science Society of America Journal*, *73*(6), 1831–1842.
618 https://doi.org/10.2136/sssaj2008.0254

Larkin, C. S., Andrews, M. G., Pearce, C. R., Yeong, K. L., Beerling, D. J., Bellamy, J., Benedick, S., Freckleton, R. P., Goring-harford, H., Sadekar, S., & James, R. H. (2022). Quantification of CO removal in a large-scale enhanced weathering field trial on an oil palm plantation in Sabah , Malaysia. *Frontiers in Climate*. https://doi.org/10.3389/fclim.2022.959229

Lei, K., Bucka, F. B., Teixeira, P. P. C., Buegger, F., Just, C., & Kögel-Knabner, I. (2025). Balancing Organic and Inorganic Carbon Dynamics in Enhanced Rock Weathering: Implications for Carbon Sequestration. *Global Change Biology*, *31*(4). https://doi.org/10.1111/gcb.70186

Leifeld, J., Zimmermann, M., & Fuhrer, J. (2008). Simulating decomposition of labile soil organic carbon: Effects of pH. *Soil Biology and Biochemistry*, *40*(12), 2948–2951. https://doi.org/10.1016/j.soilbio.2008.08.019

Lewis, A. L., Sarkar, B., Wade, P., Kemp, S. J., Hodson, M. E., Taylor, L. L., Yeong, K. L., Davies, K., Nelson, P. N., Bird, M. I., Kantola, I. B., Masters, M. D., DeLucia, E., Leake, J. R., Banwart, S. A., & Beerling, D. J. (2021). Effects of mineralogy, chemistry and physical properties of basalts on carbon capture potential and plant-nutrient element release via enhanced weathering. *Applied Geochemistry*, *132*(February), 105023. https://doi.org/10.1016/j.apgeochem.2021.105023

Manning, D. A. C., Renforth, P., Lopez-Capel, E., Robertson, S., & Ghazireh, N. (2013). Carbonate precipitation in artificial soils produced from basaltic quarry fines and composts: An opportunity for passive carbon sequestration. *International Journal of Greenhouse Gas Control*, *17*, 309–317. https://doi.org/10.1016/j.ijggc.2013.05.012

Mcbride, A. L., Wade, P., Betz, J., Stubbs, A., Bierowiec, T., Albahri, T., Cazzagon, G., Chen, C., Frew, A., Healey, M., Idam, I., Jones, L., Kelland, M. E., Mann, J., Manning, D., Mitchell, C., Murphy, M. J., Radkova, A., Tostevin, R., … Wilkie, M. (2025). *Quantifying potential carbon dioxide removal via enhanced weathering using porewater from a field trial in Scotland*. *September*. https://doi.org/10.3389/fclim.2025.1606574

Niron, H., Vienne, A., Frings, P., Poetra, R., & Vicca, S. (2024). Exploring the synergy of enhanced weathering and Bacillus subtilis: A promising strategy for sustainable agriculture. *Global Change Biology*, *30*(9), 1–18. https://doi.org/10.1111/gcb.17511

Oelkers, E. H., Declercq, J., Saldi, G. D., Gislason, S. R., & Schott, J. (2018). Olivine dissolution rates: A critical review. *Chemical Geology*, *500*(October), 1–19. https://doi.org/10.1016/j.chemgeo.2018.10.008

Palandri, J. L., & Kharaka, Y. K. (2004). A compilation of rate parameters of water-mineral interaction kinetics for application to geochemical modeling. *USGS Open File Report*, *2004–1068*, 71. http://www.dtic.mil/cgi-bin/GetTRDoc?Location=U2&doc=GetTRDoc.pdf&AD=ADA440035

Pogge von Strandmann, P. A. E., He, X., Zhou, Y., & Wilson, D. J. (2025). Comparing open versus closed system weathering experiments using lithium isotopes. *Applied Geochemistry*, *189*(July 2024), 106458. https://doi.org/10.1016/j.apgeochem.2025.106458

Pogge von Strandmann, P. A. E., Renforth, P., West, A. J., Murphy, M. J., Luu, T. H., & Henderson, G. M. (2021). The lithium and magnesium isotope signature of olivine dissolution in soil experiments. *Chemical Geology*, *560*(November 2020), 120008. https://doi.org/10.1016/j.chemgeo.2020.120008

Pogge von Strandmann, P. A. E., Tooley, C., Mulders, J. J. P. A., & Renforth, P. (2022). The Dissolution of Olivine Added to Soil at 4°C: Implications for Enhanced Weathering in Cold Regions. *Frontiers in Climate*, *4*(February), 1–11. https://doi.org/10.3389/fclim.2022.827698

Renforth, P., Pogge von Strandmann, P. A. E., & Henderson, G. M. (2015). The dissolution of olivine added to soil: Implications for enhanced weathering. *Applied Geochemistry*, *61*, 109–118. https://doi.org/10.1016/j.apgeochem.2015.05.016

Rinder, T., & von Hagke, C. (2021a). Carbon dioxide removal through enhanced weathering of basalt on agricultural land - Assessing the potential in Austria. *Preprint, Submitted to Journal of Cleaner Production*, *January*, 1–40. https://doi.org/10.31223/X51G76

Rinder, T., & von Hagke, C. (2021b). The influence of particle size on the potential of enhanced basalt weathering for carbon dioxide removal - Insights from a regional assessment. *Journal of Cleaner Production*, *315*(January), 128178. https://doi.org/10.1016/j.jclepro.2021.128178

Roland, M., Vicca, S., Bahn, M., Ladreiter-Knauss, T., Schmitt, M., & Janssens, I. A. (2015). Importance of nondiffusive transport for soil CO2 efflux in a temperate mountain grassland. *Journal of Geophysical Research: Biogeosciences*, *120*(3), 502–512. https://doi.org/10.1002/2014JG002788

Schuiling, R. D., & Krijgsman, P. (2006). Enhanced weathering: An effective and cheap tool to sequester CO 2. *Climatic Change*, *74*(1–3), 349–354. https://doi.org/10.1007/s10584-005-3485-y

Schwartz, M. O. (2022). Modelling a basalt reactor for direct air CO2 capture. *Environmental Earth Sciences*, *81*(7), 1–9. https://doi.org/10.1007/s12665-022-10320-0

Sierra, C. A., Trumbore, S. E., Davidson, E. A., Vicca, S., & Janssens, I. (2015). Sensitivity of decomposition rates of soil organic matter with respect to simultaneous changes in temperature and moisture. *Journal of Advances in Modeling Earth Systems*, *7*(1), 335–356. https://doi.org/10.1002/2014MS000358

Sohng, J., Sokol, N. W., Whiteaker, S., Schmidt, R., Holzer, I., Goertzen, H., Peña, J., Houlton, B. Z., Montañez, I., O'Geen, A., & Scow, K. (2025). Combining organic amendments with enhanced rock weathering shifts soil carbon storage in croplands. *Science of the Total Environment*, *998*(July). https://doi.org/10.1016/j.scitotenv.2025.180179

Sokol, N. W., Sohng, J., Moreland, K., Slessarev, E., Goertzen, H., Schmidt, R., Samaddar, S., Holzer, I., Almaraz, M., Geoghegan, E., Houlton, B., Montañez, I., Pett-Ridge, J., & Scow, K. (2024). Reduced accrual of mineral-associated organic matter after two years of enhanced rock weathering in cropland soils, though no net losses of soil organic carbon. *Biogeochemistry Letters*, *167*(8), 989–1005. https://doi.org/10.1007/s10533-024-01160-0

Steinwidder, L., Boito, Lucilla de Schutter, Anthony Frings, Patrick J. Miladinović, Nina Niron, Harun Rijnders, Jet Roussard, Jasper van Acker, K., van Gerven, T., & Vienne, Arthur Watjanatepin, Ponnapat Vicca, S. (2026). Higher inorganic CO2 removal despite slower weathering in an enhanced weathering experiment with steel slags and basalt (in Press.). *Global Change Biology*, *23*(1). https://doi.org/10.1111/gcb.70666

Steinwidder, L., Boito, L., Frings, P. J., Niron, H., Rijnders, J., de Schutter, A., Vienne, A., & Vicca, S. (2025). Beyond Inorganic C: Soil Organic C as a Key Pathway for Carbon Sequestration in Enhanced Weathering. *Global Change Biology*, *31*(7). https://doi.org/10.1111/gcb.70340

Strefler, J., Amann, T., Bauer, N., Kriegler, E., & Hartmann, J. (2018). Potential and costs of carbon dioxide removal by enhanced weathering of rocks. *Environmental Research Letters*, *13*(3). https://doi.org/10.1088/1748-9326/aaa9c4

Vicca, S., Goll, D., Hagens, M., Hartmann, J., Janssens, I. A., Neubeck, A., Peñuelas, J., Poblador, S., Rijnders,

J., Sardans, J., Struyf, E., Swoboda, P., van Groenigen, J. W., Vienne, A., & Verbruggen, E. (2022). Is the climate change mitigation effect of enhanced silicate weathering governed by biological processes? *Global Change Biology*, *July*, 1–16. https://doi.org/10.1111/gcb.15993

Vienne, A., Frings, P., Poblador, S., Steinwidder, L., Rijnders, J., Schoelynck, J., Vinduskova, O., & Vicca, S. (2024). Earthworms in an enhanced weathering mesocosm experiment : Effects on soil carbon sequestration , base cation exchange and soil CO 2 efflux. *Soil Biology and Biochemistry*, *199*(June), 109596. https://doi.org/10.1016/j.soilbio.2024.109596

Vienne, A., Poblador, S., Portillo-estrada, M., Hartmann, J., Ijiehon, S., Wade, P., & Vicca, S. (2022). Enhanced Weathering Using Basalt Rock Powder : Carbon Sequestration , Co-benefits and Risks in a Mesocosm Study With Solanum tuberosum. *Frontiers in Climate*, *4*(May), 1–14. https://doi.org/10.3389/fclim.2022.869456

Wagai, R., Mayer, L. M., Kitayama, K., & Shirato, Y. (2013). Association of organic matter with iron and aluminum across a range of soils determined via selective dissolution techniques coupled with dissolved nitrogen analysis. *Biogeochemistry*, *112*(1–3), 95–109. https://doi.org/10.1007/s10533-011-9652-5

Xu, T., Li, H., Vicca, S., Goll, D. S., Yang, Z., Wang, X., & Yuan, Z. (2025). *Enhanced Rock Weathering Promotes Soil Organic Carbon Accumulation : A Global Meta- - Analysis Based on Experimental Evidence*. https://doi.org/10.1111/gcb.70483

Xu, T., Yuan, Z., Vicca, S., Goll, D. S., Li, G., Lin, L., Chen, H., Bi, B., Chen, Q., Li, C., Wang, X., Wang, C., Hao, Z., Fang, Y., & Beerling, D. J. (2024). Enhanced silicate weathering accelerates forest carbon sequestration by stimulating the soil mineral carbon pump. *Global Change Biology*, *30*(8), 1–17. https://doi.org/10.1111/gcb.17464

Zhang, Y., Lavallee, J. M., Robertson, A. D., Even, R., Ogle, S. M., Paustian, K., & Cotrufo, M. F. (2021). Simulating measurable ecosystem carbon and nitrogen dynamics with the mechanistically defined MEMS 2.0 model. *Biogeosciences*, *18*(10), 3147–3171. https://doi.org/10.5194/bg-18-3147-2021

Supplementary information

1. Soil water content and temperature

While temperature was the same in every treatment, moisture was significantly affected by rock amendment. Basalt significantly increased SWC ($p<0.01$), both in the basalt-only and 3% SOC datasets. In the 3% SOC dataset there was a significantly positive basalt x time interaction effect ($p<0.01$) as well as a significantly positive dunite x time interaction on SWC ($p<0.01$), indicating that these silicates gradually increased SWC. .

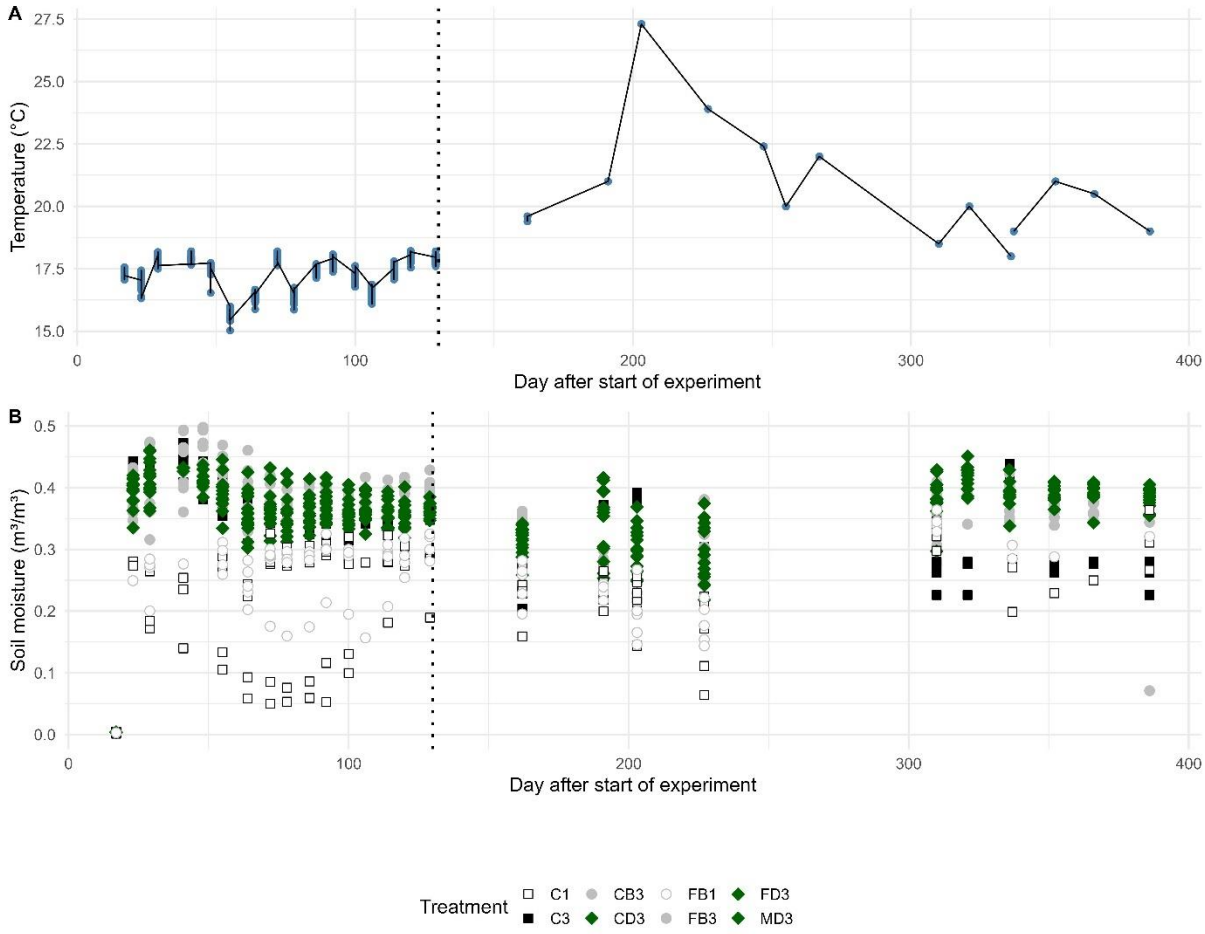

Fig. S1: (A) Experimental temperature and (B) soil moisture at every moment of SCE measurements. Before day 130 (dotted vertical line) a temperature and moisture sensor was installed in every mesocosm. After day 130 temperature and SWC were measured manually. The data gap for SWC between day 227 and day 310was due to technical problems.

2. Water inputs and leachates

Table S1: irrigation water elemental composition (average values, in mg/L).

N	Ca	Mg	Na	K	Fe	Al	Si	Ni	P	Mn	Cr
0.911	22.77882	1.301343	6.327669	12.28209	0.037757	0.129011	2.109618	0.001285	0.305199	<0.001	0.000941

3. Extended leachate data

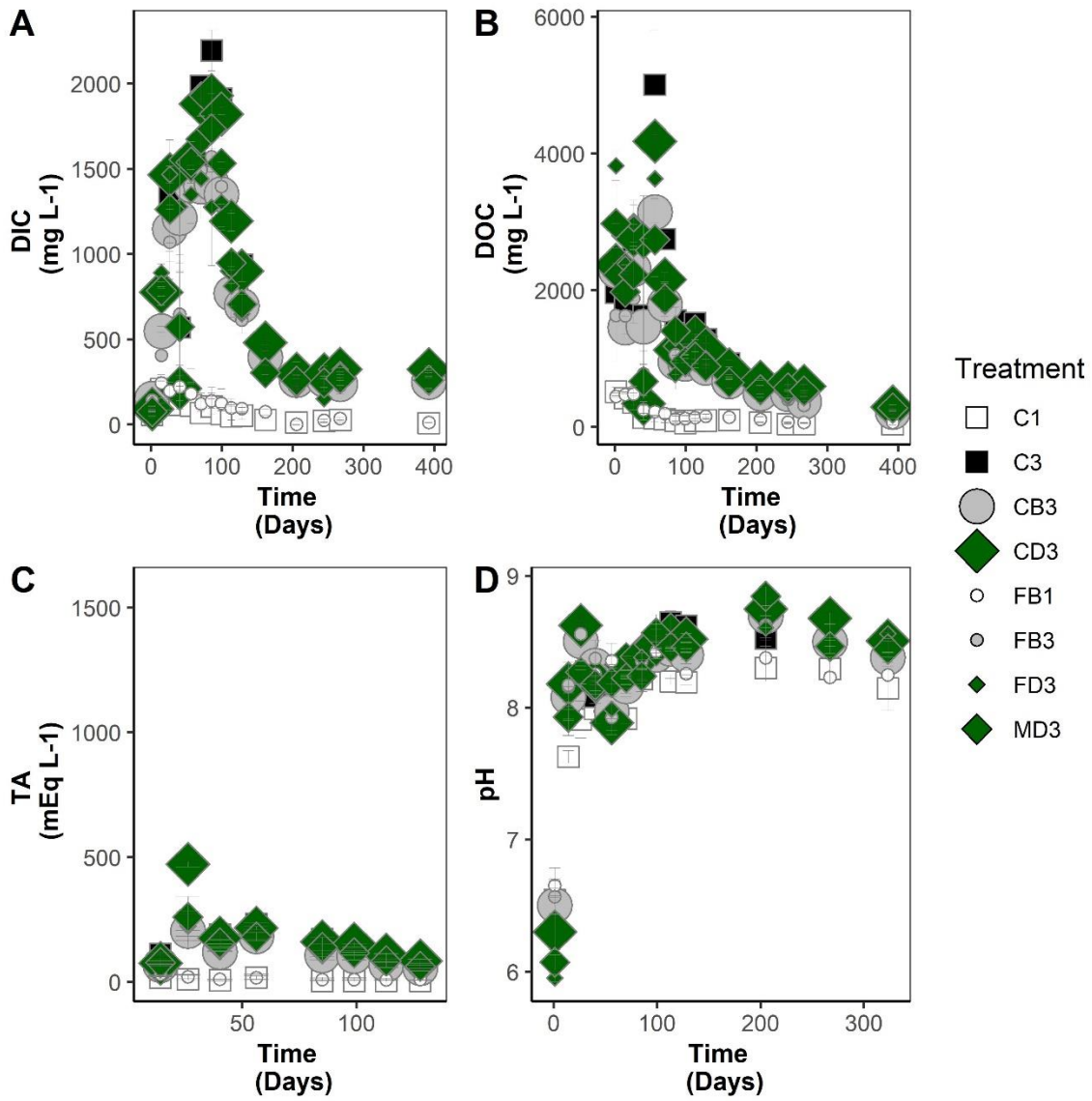

Fig. S2: Leachate composition for (A) DIC, (B) DOC, (C) TA and (D) pH in function of time for different treatments. Points and error bars indicate averages ± standard errors of the mean for all experimental data.

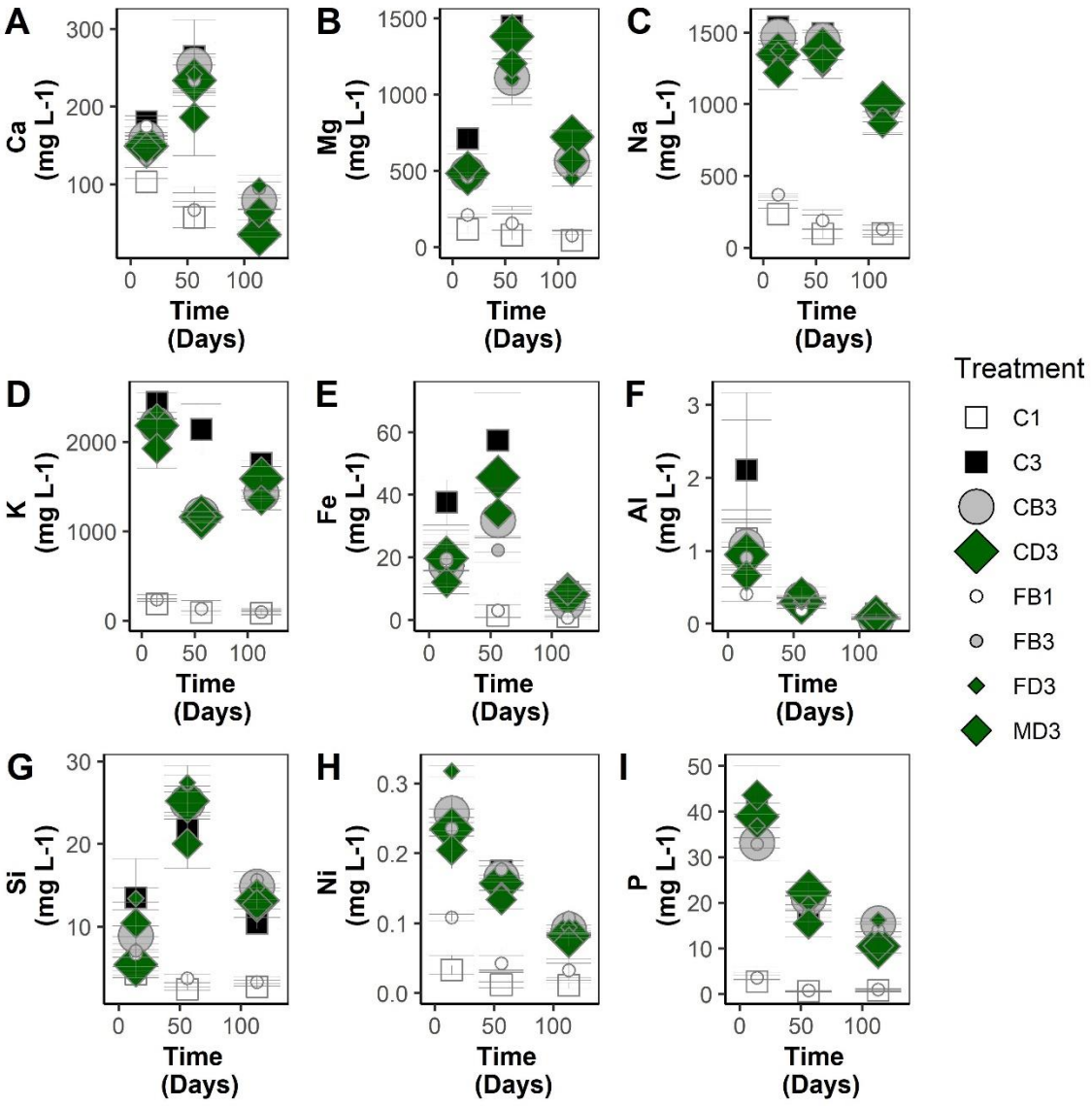

Fig. S3: Leachate composition for (A) Ca (B) Mg (C) Na (D) K (E) Fe (F) Al (G) Si (H) Ni and (I) P in function of time for different treatments. Points and error bars indicate averages ± standard errors of the mean.

Table S2: Summary statistics for masses of elements leached. All units are in mg, except TA, which is in meq. Reported values are model coefficients with p-valuesd from repeated measures linear models in parentheses. Significant effects are shown in bold. For the SOC × basalt and time x basalt interaction, p-values are only shown when significant; non-significant interaction terms were removed from the final model (indicated with N.S.).

	Treatments in dataset: C3, FB3, CB3, FD3, MD3, CD3						Treatments in dataset: C1, FB1, C3, FB3			
variable	**Basalt**	**Basalt particle size**	**Basalt x Time**	**Dunite**	**Dunite particle size**	**Dunite x Time**	**Basalt**	**Basalt x Time**	**SOC**	**SOC x Basalt**
DIC	40.18 (0.97)	-0.26 (0.41)	N.S.	-21.6 (0.98)	0 (0.97)	N.S.	-6.12 (0.93)	N.S.	**290.92 (<0.01)**	N.S.
DOC	-444.41 (0.64)	-0.15 (0.85)	N.S.	-259.4 (0.68)	-0.05 (0.86)	N.S.	-218.32 (0.22)	N.S.	**512.12 (<0.01)**	N.S.
TA	-25.44 (0.8)	-0.06 (0.39)	N.S.	-40.96 (0.24)	0.03 (0.29)	N.S.	-18.13 (0.2)	N.S.	**52.69 (<0.01)**	N.S.
Ca	-30.67 (0.96)	-0.01 (0.95)	N.S.	-45.43 (0.81)	-0.01 (0.91)	N.S.	4.01 (0.93)	N.S.	**62.64 (<0.01)**	N.S.
Mg	-272.91 (0.87)	-0.19 (0.83)	N.S.	-402 (0.49)	0.22 (0.53)	N.S.	-119.33 (0.53)	N.S.	**475.8 (<0.01)**	N.S.
Na	-224.87 (0.91)	-0.03 (0.97)	N.S.	-334.65 (0.59)	0.12 (0.73)	N.S.	-56.81 (0.77)	N.S.	**620.74 (<0.01)**	N.S.
K	-833.03 (0.19)	-0.24 (0.76)	N.S.	**-829.5 (0.02)**	0.01 (0.97)	N.S.	513.9 (0.06)	N.S.	**1120.5 (<0.01)**	**-472.03 (0.03)**
Fe	-30.26 (0.31)	0.01 (0.86)	N.S.	-26.67 (0.11)	0.01 (0.41)	N.S.	+16.70 (0.09)	N.S.	**13.01 (<0.01)**	**-15.08 (0.05)**
Al	**-1.00 (<0.01)**	-5 e-5 (0.83)	0.010 (<0.01)	**-1.02 (<0.01)**	+5e-5 (0.61)	0.010 (<0.01)	**-0.94 (<0.01)**	**0.009 (<0.01)**	0.09 (0.09)	N.S.
Si	6.09 (0.86)	-0.01 (0.63)	N.S.	1.23 (0.98)	0 (0.75)	N.S.	2.52 (0.53)	N.S.	**8.48 (<0.01)**	N.S.
Ni	0 (1)	0 (0.66)	N.S.	-0.02 (0.85)	0 (0.76)	N.S.	0.02 (0.5)	N.S.	**0.07 (<0.01)**	N.S.
P	-4.85 (0.85)	0 (0.92)	N.S.	-1.91 (0.94)	0 (0.75)	N.S.	-1.75 (0.53)	N.S.	**10.85 (<0.01)**	N.S.

4. Extended mesh bag (pure silicate) data

Solid inorganic carbon (SIC) in basalt or dunite powders in mesh bags was quantified using a Scheibler calcimeter (Model 08.53, Royal Eijkelkamp, Giesbeek, The Netherlands), calibrated with 2–400 mg $CaCO_3$ based on CO_2 released after adding 4 M HCl. SIC was determined from 3 g dry rock powdered as in **Equation 1**.

$$Calcimetry:$$

$$SIC\ [\%] = \frac{\left(Callibration\ intercept\ [mL] + \ delta\ V_{CO2}[mL] * Callibration\ Slope\ \left[\frac{gCaCO3}{mL\ CO2}\right]\right) * \frac{12}{100}\left[\frac{gSIC}{g\ CaCO3}\right] * 100}{3\ [g\ soil]} \quad (1)$$

The change in SIC (ΔSIC) was calculated from the difference in in SIC between original rock powder and mesh bag samples taken on day 119. The ΔSIC was significantly more negative for dunite than for basalt (**Fig S4**). The finer the dunite, the more SIC decreased. We observed a positive effect of SOC on ΔSIC, but ΔSIC of silicates in mesh bags remained negative for every rock type. The positive effect of SOC on SIC is most likely due to the carbonates in the manure.

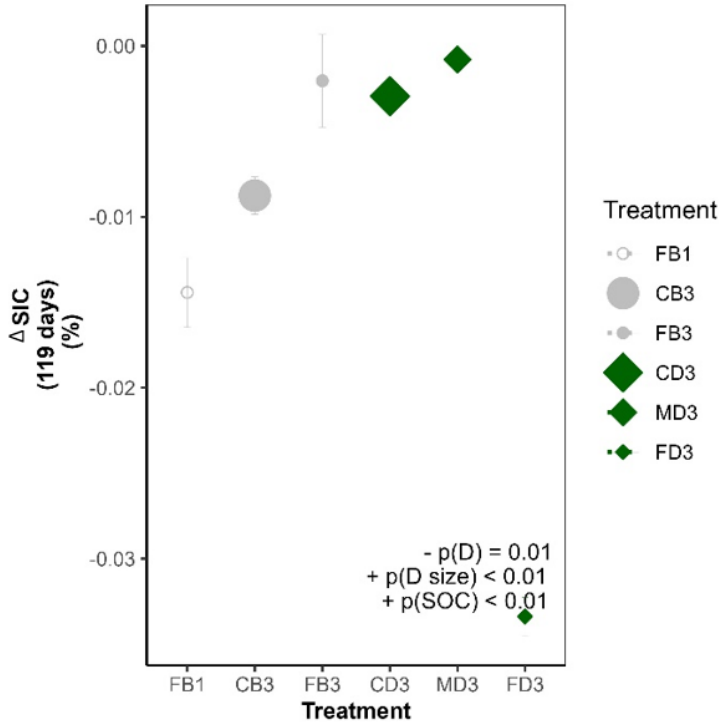

Fig. S4: Change in SIC change in time (ΔSIC; over 119 days) in silicate mesh bags.

5. 'Heckman' extractions

As an additional analysis to investigate the 'organo-minerallic glue' formation hypothesis in basalt soils, We performed a second sequential extraction protocol, following Heckman et al. (2018). These extractions were done on all basalt amended soils on day 130, and on all soils at day 389. These Heckman extractions allow us to distinguish between the pyrophosphate-, NH_2OH- and dithionite-extractable pools. Pyrophosphate and hydroxylamine fractions are associated with amorphous minerals, while dithionite is associated with crystalline minerals. The Heckman extractions revealed that both amorphous and crystalline Fe hydroxides were formed. Oxidized Al, Ca, Mg and Si increases were observed in amorphous fractions but not in crystalline (dithionite extracted) fractions (Fig. S5 and S6).

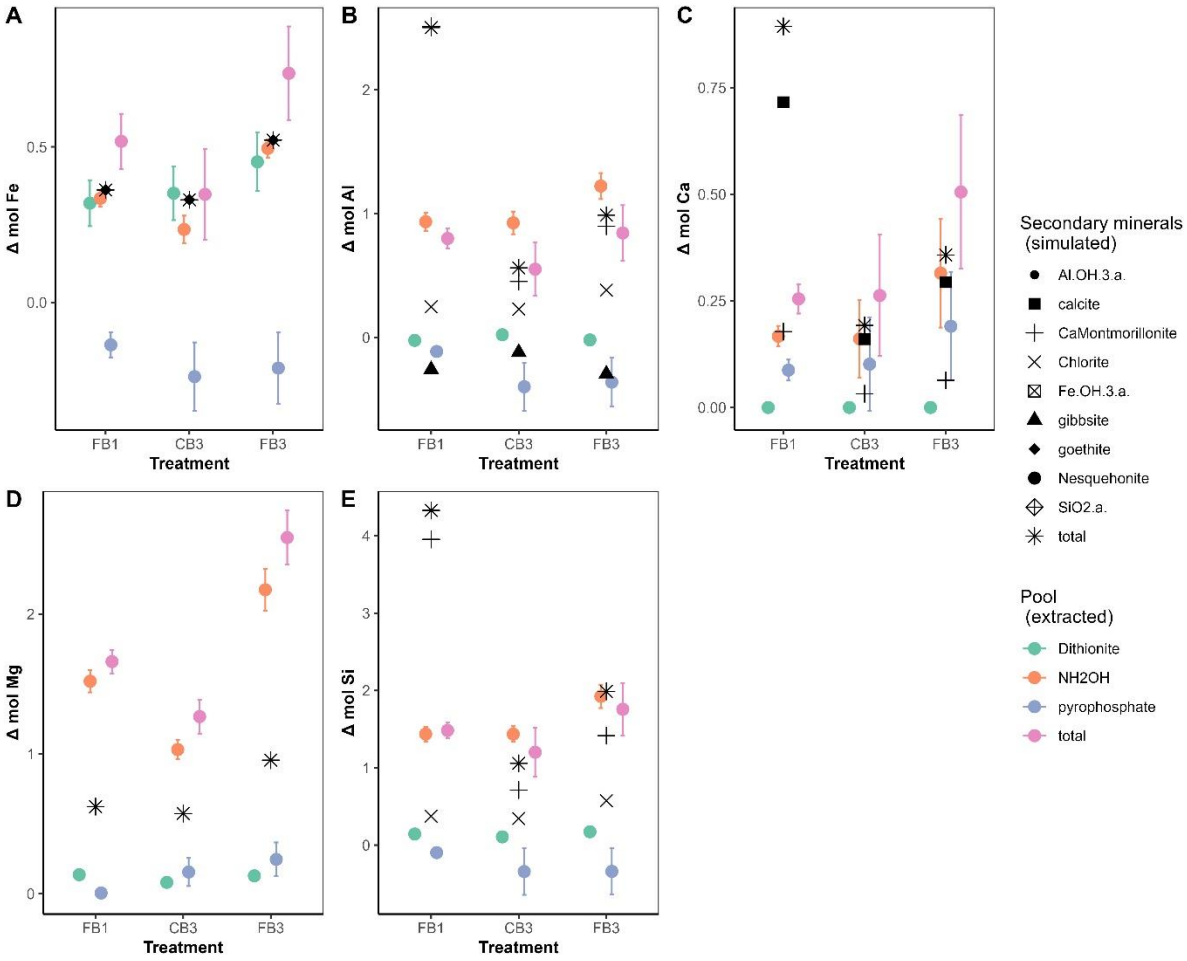

Fig. S5: Change in elements in extracted soil pools after 130 days (Heckman extractions, colored symbols) for each treatment, relative to control soils and comparison with simulated secondary minerals (black symbols, stars are the total change) for (A) Fe, (B) Al, (C) Ca, (D) Mg, (E) Si. Only secondary minerals that were formed according to the model are included. Colored symbols and error bars show experimental averages and standard errors of the mean. An overview of statistical changes for the dataset with treatments (C1, C3, FB1 and FB3) is shown in **Table S3.**

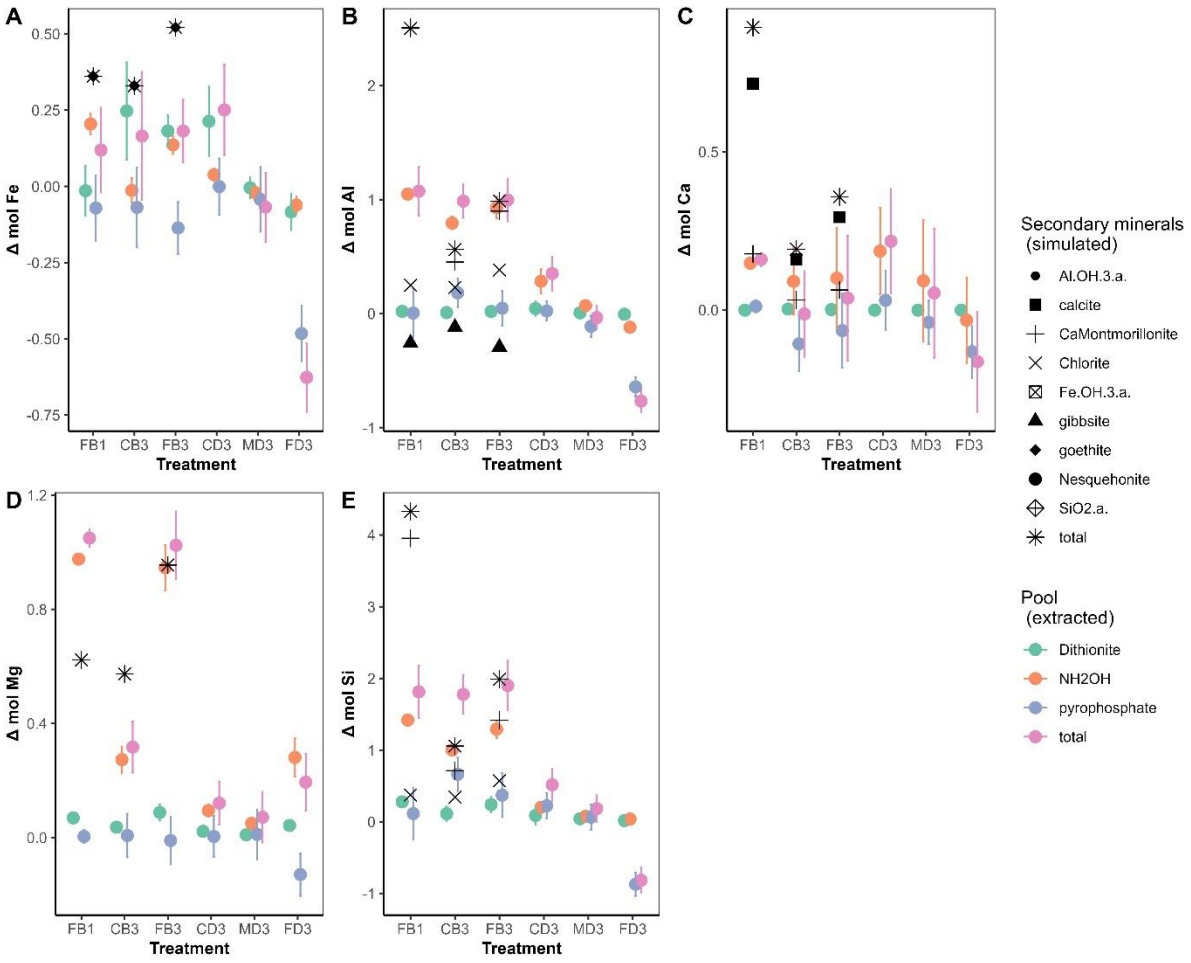

Fig. S6: Change in elements in extracted soil pools after 389 days (Heckman extractions, colored symbols) for each treatment, relative to control soils and comparison with simulated secondary minerals (black symbols, stars are the total change) for (A) Fe, (B) Al, (C) Ca, (D) Mg, (E) Si. Only secondary minerals that were formed according to the model are included. Colored symbols and error bars show experimental averages and standard errors of the mean. An overview of statistical changes for the dataset with treatments (C1, C3, FB1 and FB3) is shown in **Table S3.**

Table S3: Statistic results for changes in elemental content in Heckman extracted soil pools, fitted against SOC, basalt and interaction effects for a dataset with control soil and fine basalt. All basalt x SOC interaction effects were not statistically significant. Significant basalt effects are indicated in bold. For the SOC × basalt, p-values are only shown when significant; non-significant interaction terms were removed from the final model (indicated with N.S.). These statistical tests were performed on the dataset with treatments (C1, C3, FB1 and FB3) and a repeated measures Anova was used with data from both day 130 and 389.

pool	element	Basalt	SOC	SOC x Basalt	P (basalt)	P (SOC)	P (basalt x SOC)
pyrophosphate	Fe	-1.1e-01	1.1e-01	-1e-01	0.08	**<0.01**	N.S.
pyrophosphate	Al	-1.1e-01	2.7e-02	-1e-01	0.3	0.61	N.S.

pool	element	Basalt	SOC	SOC x Basalt	P (basalt)	P (SOC)	P (basalt x SOC)
pyrophosphate	Ca	-5.2e-02	2.7e-01	-1e-01	0.64	<**0.01**	N.S.
pyrophosphate	Mg	-5.2e-02	2.3e-01	-1e-01	0.6	<**0.01**	N.S.
pyrophosphate	Si	5.5e-02	1.8e-01	-1e-01	0.81	0.12	N.S.
NH2OH	**Fe**	2.1e-01	-3e-02	-1e-01	<**0.01**	0.34	N.S.
NH2OH	**Al**	7.1e-01	-8.9e-02	-1e-01	<**0.01**	0.29	N.S.
NH2OH	**Ca**	1.7e-01	1.8e-01	-1e-01	<**0.01**	<**0.01**	N.S.
NH2OH	**Mg**	1e+00	-1.3e-01	-1e-01	<**0.01**	0.27	N.S.
NH2OH	**Si**	1e+00	-2.1e-01	-1e-01	<**0.01**	0.12	N.S.
Dithionite	**Fe**	1.8e-01	-2.6e-02	-1e-01	<**0.01**	0.42	N.S.
Dithionite	Al	1.1e-02	2.7e-02	-1e-01	0.55	<**0.01**	N.S.
Dithionite	Ca	1.1e-02	5.1e-03	-1e-01	0.11	0.14	N.S.
Dithionite	**Mg**	8.9e-02	-3.4e-03	-1e-01	<**0.01**	0.63	N.S.
Dithionite	**Si**	1.9e-01	4.1e-02	-1e-01	<**0.01**	0.05	N.S.

830

831

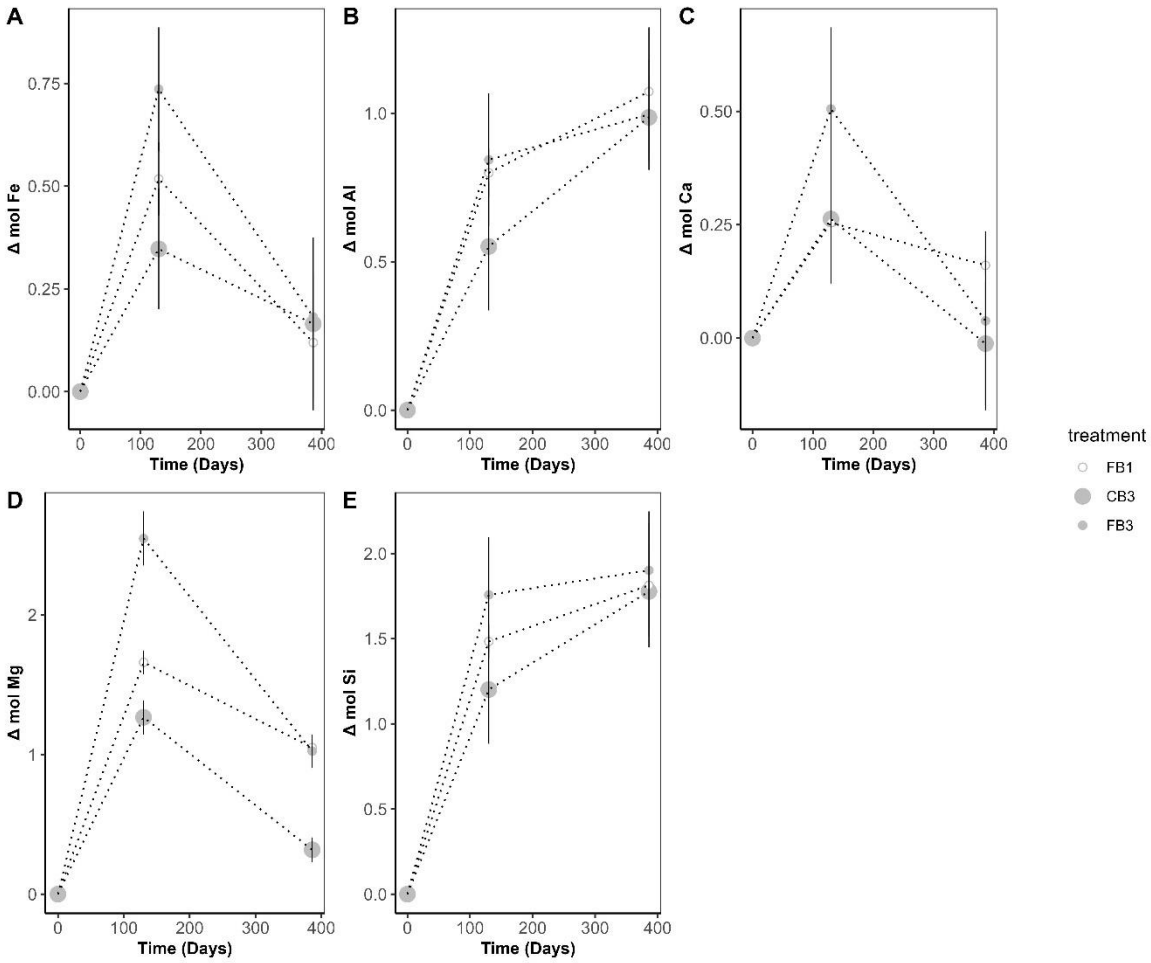

Fig. S7: The change in elements (A) Fe (B) Al (C) Ca (D) Mg and (E) Si (total of the Heckman extracted pools) relative to control soils, in function of time after rock amendment for basalt treatments.

6. Model – SCE data comparison and SOM decomposition

For control soils, we could recreate the temporal dynamics for cumulative SCE relatively well (**Fig. S8**), while we could not simulate temporal dynamics for silicate amended soils. We the same parameterization to both the 1% and 3% SOC soil models and retained the parameter set that best fit the 3% SOC model (panel B below).

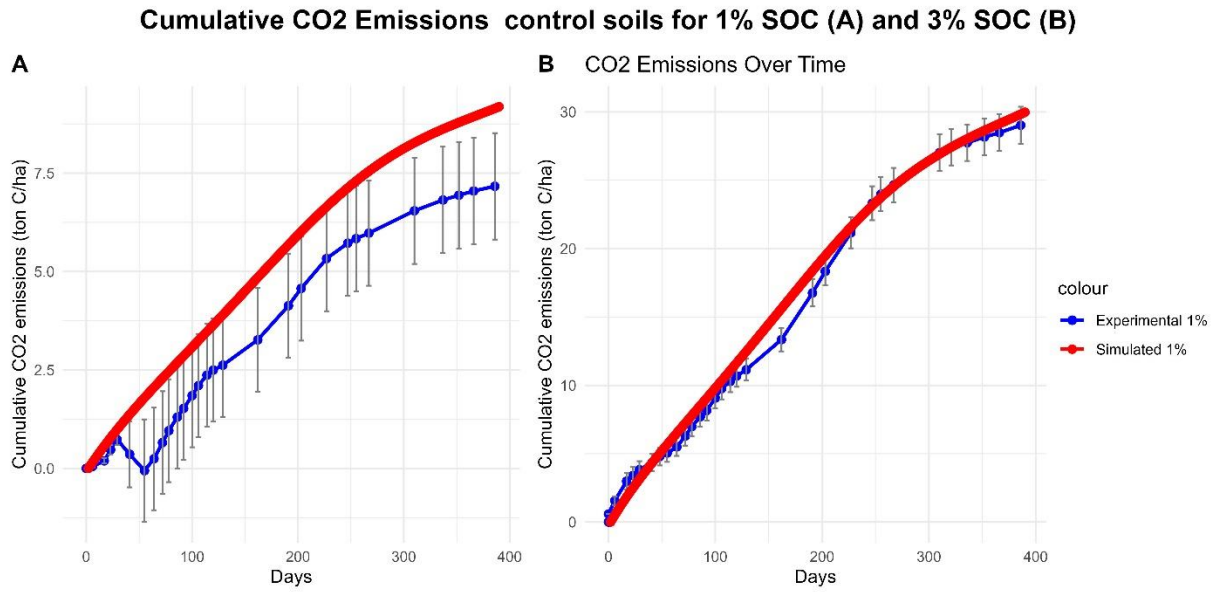

Fig. S8: Control simulation versus experimental comparison: Experimental and simulated SCE for (A) 1% SOC control soil and (B) the 3% SOC soil.

Temporal differences between SCE in control and amended soils are shown in **Fig. S9.**

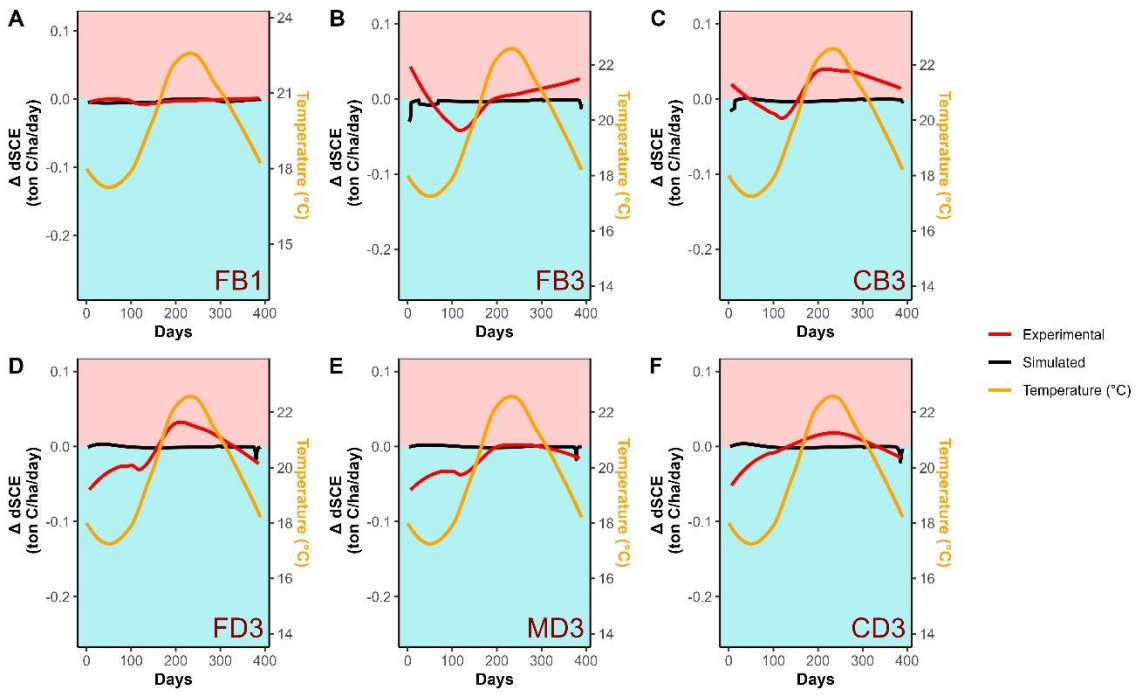

Fig. S9: Temporal evolution of experimental and simulated changes for ΔSCE (the difference in SCE between a treatment and its control treatment) for each treatment (A) FB1 (B) FB3 (C) CB3 (D) FD3 (E) MD3 and (F) CD3 The light blue area indicates periods when rock-amended mesocosms emitted less CO_2 than controls, while the pink area indicates periods when rock-amended soils emitted more CO_2. Temperature is shown in orange on the secondary axis for comparison.

Decomposition fluctuated among treatments due to minor fluctuations in pH. In the 1% soils, the relatively lower SCE and thus pCO_2, combined with the high alkalinity in the control, led to a control pH that exceeded 8. Consequently, basalt amendment did not further increase pH. In the 3%, the higher SCE reflects a higher pCO_2 and thus a lower control pH of 7-7.5. Under these conditions, basalt amendment increased pH above 8 and thus stimulated decomposition (which is maximal at 8 according to the Leifeld relationship). The SWC was first normalized by total porosity (calculated from bulk density) and the moisture modifier was modelled using the Gompertz relationship (see Table 2 of (Sierra et al., 2015). The SWC modifier was 1 in all treatments during this experiment as water was not limiting decomposition. Temperature was equal in all amended/unamended treatments so that the temperature modifier did not change, The total decomposition modifier thus overlaps with the pH modifier (in red; **Fig. S10).** Overall, decomposition modifiers were not substantially affected by our treatments.

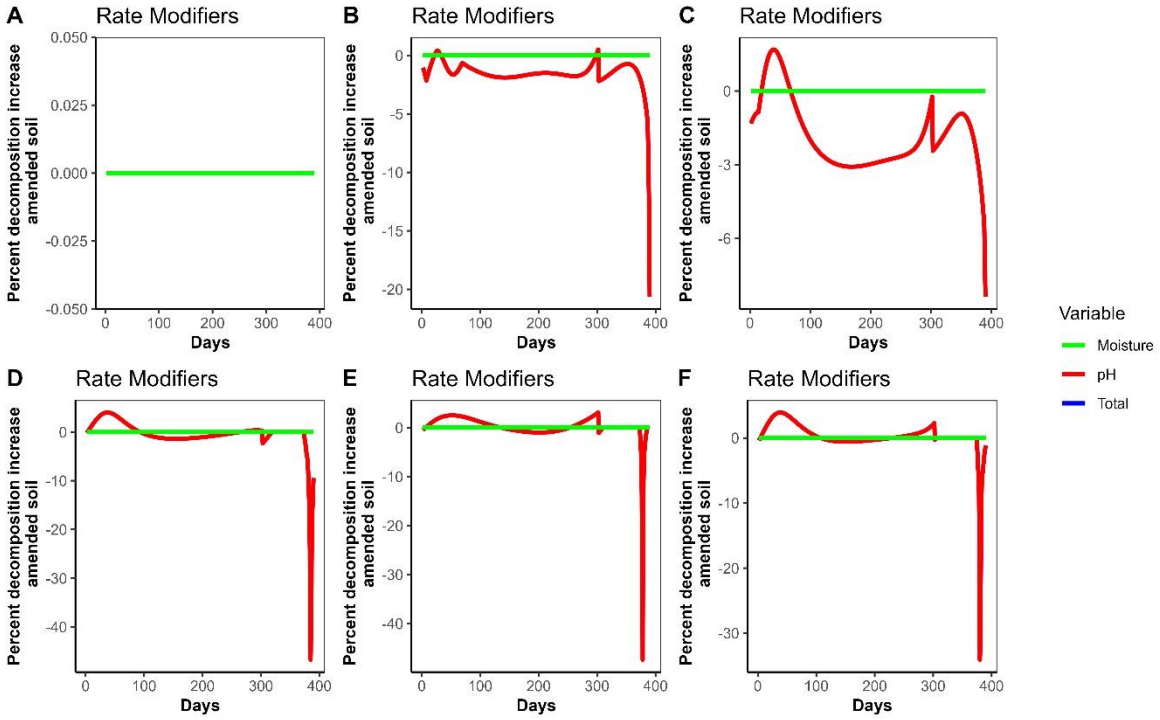

Fig. S10: Decomposition rate modifiers for treatments (A) FB1 (B) FB3 (C) CB3 (D) CD3 (E) MD3 and (F) FD3. Note that the green line is 0 everywhere (as the moisture rate modifier was equal in (un)amended soils) and that the red pH modifier overlaps with the total change in decomposition (blue, not visible) of amended relative to control soil.

Besides changes in decomposition, also MAOM-C formed by adsorption of DOC to Fe and Al hydroxides (**Fig. S11).** In addition, clays were formed that decreased the ratio of actively/slowly decomposing SOC, leading to an increase in SOC relative in basalt amended soils relative to control soils.

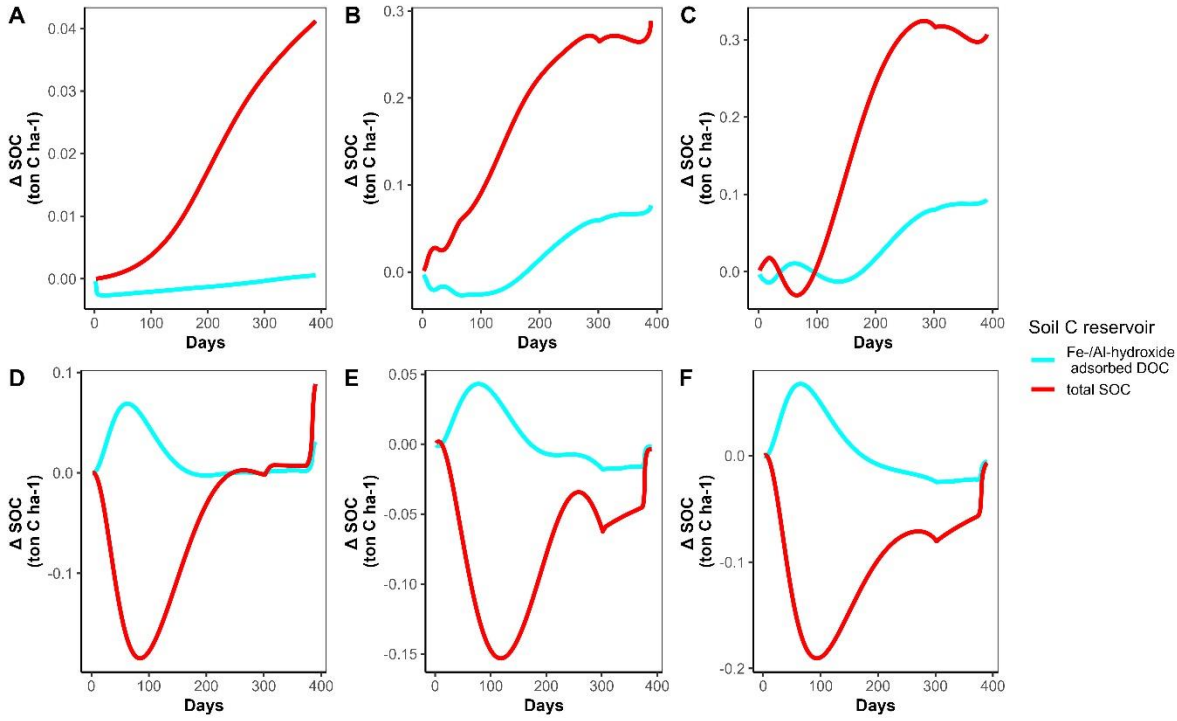

Fig. S11: Change in SOC and adsorbed DOC (=MAOM-C) in amended soils relative to controls for treatments (A) FB1 (B) FB3 (C) CB3 (D) CD3 (E) MD3 and (F) FD3. Total SOC change is affected by MAOM-C, but also by changes in pH modifiers and clay content (which affects the ratio of slow/actively SOC degradation) among treatments.

7. Particle size distribution rock powders

Table S4: Particle size distribution of dunite and basalt.

Size fraction	Fine basalt (%)	Coarse basalt (%)	Fine dunite (%)	Mid-size dunite (%)	Coarse dunite (%)
< 0.010 µm	0	0	0	0	0
0.01µm-0.05µm	0	0	0	0	0

0.05µm-0.10µm	0	0	0	0	0
0.10µm-0.20µm	0	0	0	0	0
0.20µm-0.30µm	0	0	0	0	0
0.30µm-0.50µm	0.249	0	0.521	0	0
0.50µm-0.75µm	0.663	0	1.496	0	0
0.75µm-1.00µm	0.557	0	1.2	0	0
1.00µm-1.50µm	0.82	0	1.638	0	0
1.50µm-2.00µm	0.679	0	1.384	0	0
2.00µm-4.00µm	2.141	0	5.204	0.21	0
4.00µm-8.00µm	3.13	0	9.142	0.469	0
8.00µm-16.00µm	4.523	0	15.485	0.335	0
16.00µm-30.00µm	5.472	0	18.61	0.9	0
30.00µm-45.00µm	4.698	0	12.436	0.329	0
45.00µm-60.00µm	4.12	0	8.421	0	0
60.00µm-75.00µm	3.82	0	6.082	-0.005	0
75.00µm-90.00µm	3.709	0	4.515	0.478	0
90.00µm-105.00µm	3.709	0	3.381	2.031	0
105.00µm-120.00µm	3.753	0	2.537	3.937	0
120.00µm-135.00µm	3.793	0	1.908	5.697	0

135.00µm-150.00µm	3.809	0	1.433	7.055	0
150.00µm-165.00µm	3.781	0	1.081	7.876	0
165.00µm-180.00µm	3.716	0.009	0.816	8.212	0
180.00µm-200.00µm	4.781	0.359	0.792	10.766	0
200.00µm-220.00µm	4.518	1.013	0.543	9.955	0
220.00µm-240.00µm	4.202	1.679	0.367	8.783	0
240.00µm-260.00µm	3.858	2.317	0.237	7.452	0
260.00µm-280.00µm	3.503	2.868	0.153	6.161	0
280.00µm-300.00µm	3.149	3.35	0.1	4.952	0.038
300.00µm-330.00µm	4.09	5.705	0.102	5.521	0.437
330.00µm-360.00µm	3.394	6.251	0.081	3.717	1.107
360.00µm-400.00µm	3.572	8.755	0.088	2.996	2.5
400.00µm-450.00µm	3.22	10.901	0.091	1.728	4.544
450.00µm-500.00µm	2.16	10.253	0.073	0.434	5.833
500.00µm-550.00µm	1.39	9.223	0.055	0.013	6.728
550.00µm-600.00µm	0.748	8.028	0.029	0	7.225
600.00µm-650.00µm	0.244	6.806	0	0	7.399
650.00µm-700.00µm	0.029	5.65	0	0	7.302
700.00µm-750.00µm	0	4.596	0	0	7.014

750.00µm-800.00µm	0	3.645	0	0	6.586
800.00µm-850.00µm	0	2.836	0	0	6.072
850.00µm-900.00µm	0	2.145	0	0	5.509
900.00µm-950.00µm	0	1.604	0	0	4.939
950.00µm-1000.00µm	0	1.13	0	0	4.374
1000.00µm-2000.00µm	0	0.876	0	0	22.394

887

888

889

890